Check for updates

AGU ADVANCING EARTH AND SPACE SCIENCES

AGU Advances

RESEARCH ARTICLE
10.1029/2026AV002407

Abrupt Onset and Persistent Downstream Effects of Acid Rock Drainage on Rivers Across Northwest Arctic Alaska

Taylor G. Evinger[1], Jonathan A. O'Donnell[2], Michael P. Carey[3], Joshua C. Koch[3], Carson A. Baughman[3], Kenneth R. Hill[4], Rebecca J. Frei[1], and Brett A. Poulin[1]

[1]Department of Environmental Toxicology, University of California Davis, Davis, CA, USA, [2]National Park Service, Arctic Network, Anchorage, AK, USA, [3]U.S. Geological Survey, Alaska Science Center, Anchorage, AK, USA, [4]National Park Service, Arctic and Central Alaska Networks, Fairbanks, AK, USA

Peer Review The peer review history for this article is available as a PDF in the Supporting Information.

Key Points:

- Acid rock drainage sources have low pH and elevated sulfate and metals compared to unaffected rivers and tributaries
- Mixing of acid rock drainage inputs with mainstem rivers cause sustained downstream increases in sulfate and metal concentrations
- Step-increases in sulfate and metals concentrations in 2019 point to a broad, climate-driven shift after a warm, high-snow winter

Supporting Information:

Supporting Information may be found in the online version of this article.

Correspondence to:

B. A. Poulin,
bapoulin@ucdavis.edu

Citation:

Evinger, T. G., O'Donnell, J. A., Carey, M. P., Koch, J. C., Baughman, C. A., Hill, K. R., et al. (2026). Abrupt onset and persistent downstream effects of acid rock drainage on rivers across northwest Arctic Alaska. *AGU Advances*, *7*, e2026AV002407. https://doi.org/10.1029/2026AV002407

Received 20 MAR 2026
Accepted 26 AUG 2026

Author Contributions:

Conceptualization: Taylor G. Evinger, Jonathan A. O'Donnell, Michael P. Carey, Joshua C. Koch, Carson A. Baughman, Brett A. Poulin
Data curation: Taylor G. Evinger, Jonathan A. O'Donnell, Joshua C. Koch, Carson A. Baughman, Kenneth R. Hill, Rebecca J. Frei, Brett A. Poulin
Formal analysis: Taylor G. Evinger, Joshua C. Koch, Rebecca J. Frei

© 2026. The Author(s). AGU Advances published by Wiley Periodicals LLC on behalf of American Geophysical Union. This is an open access article under the terms of the Creative Commons Attribution License, which permits use, distribution and reproduction in any medium, provided the original work is properly cited.

Abstract Arctic streams and rivers are increasingly vulnerable to degradation from permafrost thaw that releases toxic elements via natural acid rock drainage. However, the spatial and temporal evolution of acid rock drainage on river chemistry across diverse mineral settings remain poorly constrained. Here, water chemistry in six watersheds across Alaska's Brooks Range (2022–2024) quantified the effects of acid rock drainage on river chemistry. Point-source acid rock drainage inputs (seeps and impaired tributaries) exhibited lower pH (median; pH: 3.2 and 6.9, respectively), higher sulfate (SO_4^{2-}: 3,025 and 390 mg L^{-1}, respectively), and elevated major and trace element concentrations (sum of 23 metals: 451 and 9.2 mg L^{-1}, respectively), compared to upstream unimpaired mainstem rivers (pH = 8.3, SO_4^{2-} = 68 mg L^{-1}; metals = 0.1 mg L^{-1}). Across watersheds, these inputs increased mainstem concentrations of major and trace elements (e.g., Fe, Al, Mn, Zn, Ni, Cd, and rare earth elements) and SO_4^{2-}; however, mainstem river pH remained stable due to sufficient buffering. Within the Salmon River, concentrations of filter-passing and particulate fractions of constituents (SO_4^{2-}, Fe, Zn, Ni, and Cd) were elevated ≤70-fold at >100 km downstream of acidic inputs, documenting long-range transport. Temporal analyses of SO_4^{2-} and Zn concentration (2015–2024) revealed abrupt increases (≤263%) in two watersheds between 2019 and 2020, aligning with antecedent record warm and snowy winter conditions. Collectively, our results document the abrupt onset of acid rock drainage across Arctic rivers with potential for long-range downstream transport and implications for biogeochemical cycles and ecological and human health.

Plain Language Summary Warming in the Arctic is accelerating permafrost thaw, leading to changes in the water quality of streams and rivers that provide important ecosystem services to rural communities. In Arctic Alaska, a growing concern is the increasing number of rivers affected by natural acid rock drainage, a process that occurs when certain minerals are exposed to air and water, releasing acid, sulfate, and a mixture of major and trace metals. Here, we examined the effects of acid rock drainage on river chemistry across six watersheds in Alaska's Brooks Range. Acid rock drainage inputs were extremely acidic, with concentrations of nickel, zinc, and cadmium similar to those observed in mine-impacted rivers outside the region. Acidic, metal-rich inputs to rivers raised metal levels downstream by up to 70 times, with the potential for long range transport (>100 km). We used long-term water quality records to constrain the timing of onset to 2019–2020, which coincided with warm, snowy conditions of the preceding winters. Collectively, our findings document the recent and abrupt onset of acid rock drainage that releases toxic metals to Arctic rivers, with implications for wildlife and humans.

1. Introduction

The Arctic is warming four times faster than the globe as a whole (Rantanen et al., 2022), causing rapid changes to hydrology, ecology, and biogeochemical cycling in stream and river systems in high-latitude regions (Koch & O'Donnell, 2025). Arctic streams and rivers provide critical habitat for resident and anadromous fish and ecosystem services to rural communities and are vulnerable to degradation in quality from widespread permafrost thaw (Sullivan et al., 2025; Thomas et al., 2025). As permafrost thaws with warmer Arctic temperatures and increased snowfall (S. L. Smith et al., 2022), previously immobilized reservoirs of carbon (C) (Schuur et al., 2015), nutrients (Gao et al., 2018; Strauss et al., 2017), and major and trace elements (Loiko et al., 2017; Schuster et al., 2011) can be mobilized to ground and surface waters, with diverse implications for river and stream water quality (Shogren et al., 2022; Tank et al., 2023; Toohey et al., 2016). An emerging threat to Arctic rivers is the mobilization of metals due to changes in subsurface flow paths (e.g., driven by permafrost soil thaw)

Funding acquisition: Taylor G. Evinger, Jonathan A. O'Donnell, Michael P. Carey, Joshua C. Koch, Carson A. Baughman, Brett A. Poulin
Investigation: Taylor G. Evinger, Jonathan A. O'Donnell, Michael P. Carey, Joshua C. Koch, Carson A. Baughman, Brett A. Poulin
Methodology: Taylor G. Evinger, Joshua C. Koch
Project administration: Taylor G. Evinger, Jonathan A. O'Donnell, Michael P. Carey, Joshua C. Koch, Carson A. Baughman, Brett A. Poulin
Supervision: Taylor G. Evinger, Jonathan A. O'Donnell, Michael P. Carey, Joshua C. Koch, Carson A. Baughman, Brett A. Poulin
Visualization: Taylor G. Evinger, Joshua C. Koch, Carson A. Baughman, Brett A. Poulin
Writing – original draft: Taylor G. Evinger, Joshua C. Koch
Writing – review & editing: Taylor G. Evinger, Jonathan A. O'Donnell, Michael P. Carey, Joshua C. Koch, Carson A. Baughman, Kenneth R. Hill, Rebecca J. Frei, Brett A. Poulin

that enhance groundwater interactions with deeper mineral layers (Frey & McClelland, 2009; Walvoord et al., 2012), which in turn stimulate the oxidative weathering of sulfide minerals (termed acid rock drainage) (O'Donnell et al., 2024; Skierszkan et al., 2026). As of 2025, over 200 rivers and streams across Alaska's Brooks Range have been identified as potentially affected by natural acid rock drainage based on remote sensing imagery (O'Donnell et al., 2025), with similar observations of intensified sulfide mineral oxidation in Yukon, Canada (Skierszkan et al., 2026), highlighting the potential for this disturbance to alter water chemistry across the Arctic and constituent loading to the Arctic Ocean.

Enhanced acid rock drainage due to a warming climate has been documented across other Arctic (Kemeny et al., 2023; Skierszkan et al., 2026; Van Stempvoort et al., 2023), boreal (Kwong et al., 2009), and alpine environments (Crouch et al., 2013; Rue & McKnight, 2021; Todd et al., 2012), affecting river chemistry and elevating metal concentrations to potentially toxic levels. In parallel, studies on large Arctic rivers have documented substantial changes in the fluxes of nutrients and anions to the Arctic Ocean, often observed as gradual yet systematic shifts over decades (Drake et al., 2018; Tank et al., 2023; Toohey et al., 2016). For example, observed changes in dissolution of carbonates and sulfide minerals inferred from alkalinity (Drake et al., 2018) and sulfate (SO_4^{2-}) concentrations (Toohey et al., 2016) in larger Arctic rivers has implications for global carbon cycling (Zolkos et al., 2018). However, investigations within smaller watersheds document that SO_4^{2-} concentration, a byproduct of sulfide mineral weathering, can vary drastically over space and time (Skierszkan et al., 2026; Walsh et al., 2024). Preliminary assessments of changes in the chemistry of smaller watersheds in Alaska's Brooks Range support that recent metal mobilization was primarily governed by natural acid rock drainage (O'Donnell et al., 2024), as impaired rivers were more acidic and had markedly higher concentrations of filter-passing SO_4^{2-} and major and trace elements, characteristic of sulfide mineral oxidation (Alpers et al., 2003; Nordstrom & Alpers, 1999). Despite accelerated changes underway in the Arctic, and broad recognition of the importance of metal mobilization (Barker et al., 2014; O'Donnell et al., 2024; Skierszkan et al., 2024, 2026; Sullivan et al., 2025), there is limited information on (a) how the chemistry of Arctic rivers respond to acid rock drainage inputs from different mineral sources, (b) the spatial extent to which acid rock drainage constituents persist downstream, and (c) the temporal dynamics (e.g., onset and recovery) of acid rock drainage inputs.

To address these research questions, we conducted a comprehensive chemical evaluation of acid rock drainage inputs across six watersheds in Alaska's Brooks Range, including analyses of in situ conditions (e.g., pH, dissolved oxygen (DO) concentration, specific conductance) and concentrations of dissolved organic carbon (DOC), dissolved inorganic carbon (DIC) and acid-neutralizing capacity, major cations and anions, and major, trace, and rare earth elements (REE). In each watershed, point-source acid rock drainage inputs (including hillside seeps and impaired tributaries) and mainstem river or stream reaches upstream (i.e., unimpacted by acid rock drainage) and downstream of acid rock drainage inputs were sampled. We evaluated the chemical compositions of acid rock drainage inputs, benchmarked metal concentrations to acid mine drainage chemical classification, and quantified the downstream effects on water quality across the six watersheds. Lastly, we leveraged unique data sets of specific watersheds to evaluate long-range downstream transport and constrain the temporal dynamics of acid-rock drainage onset and recovery. We discuss the chemical composition, downstream persistence, and temporal dynamics in context of potential biogeochemical and toxicological implications.

2. Methods

2.1. Study Area

Six Arctic watersheds (ranging from 83 to 2,059 km^2; Table S1 in Supporting Information S1) were studied in the western Brooks Range of Alaska (Figure 1). Three of the watersheds are within Noatak National Preserve and are tributaries of the Noatak River (the Agashashok River, Kugururok River, and Nakolikurok Creek), and three watersheds were within or adjacent to Kobuk Valley National Park and tributaries of the Kobuk River (the Salmon River, Anaktok Creek, and Tukpahlearik Creek). All watersheds ultimately drain to Kotzebue Sound and the Chukchi Sea. Both the Noatak River and Salmon River are designated National Wild and Scenic Rivers (ANILCA, Public Law, 1980). The Anaktok Creek watershed is nested within the Salmon River watershed and handled as a unique subcatchment. All watersheds were underlain by continuous permafrost (Jorgenson et al., 2008), with a range of low (<10% volume), moderate (10%–40% volume), or variable ground ice content (Table S2 in Supporting Information S1). Dominant land cover of the watersheds was dwarf shrub (ranging from 42% to 69% of watershed area) and shrub (14%–36%), with smaller proportions of sedge, barren land, and

2576604x, 2026, 6, Downloaded from https://agupubs.onlinelibrary.wiley.com/doi/10.1029/2026AV002407 by Jonathan O'Donnell , Wiley Online Library on [24/09/2026]. See the Terms and Conditions (https://onlinelibrary.wiley.com/terms-and-conditions) on Wiley Online Library for rules of use; OA articles are governed by the applicable Creative Commons License

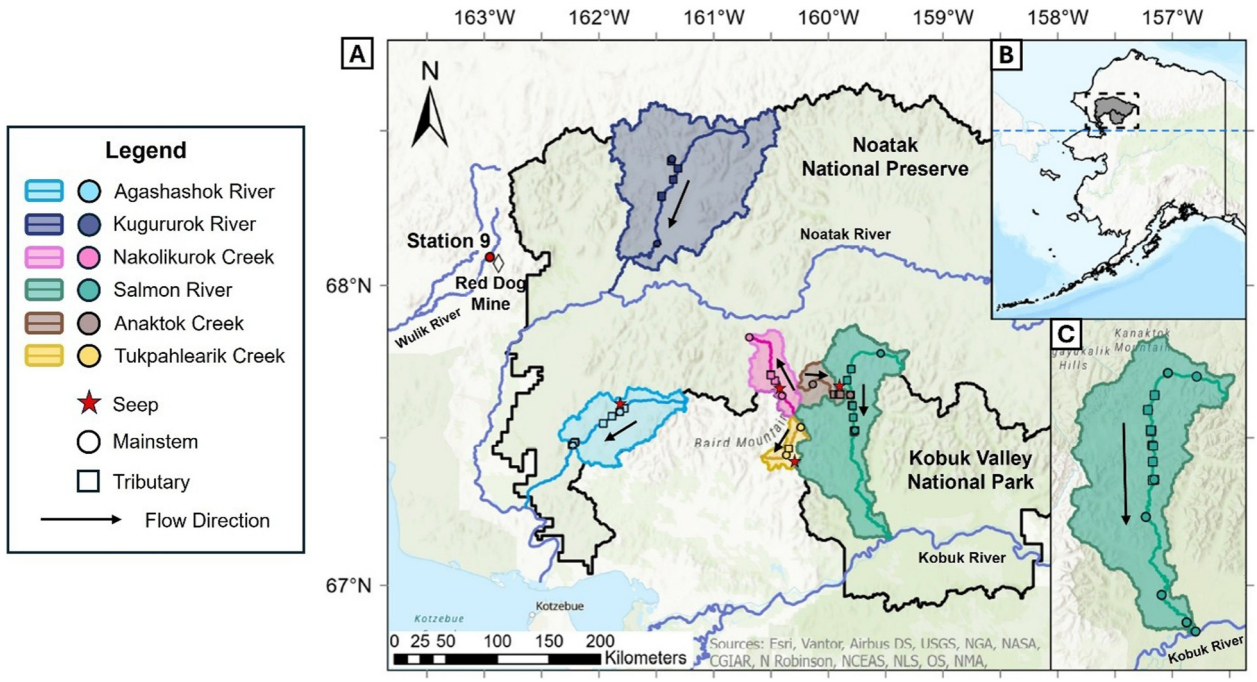


Figure 1. (a) Map of Arctic watersheds (shaded regions) and sampling locations in Noatak National Preserve and Kobuk Valley National Park (northwest Alaska). Markers identify sampling locations of surface waters. Diamonds identify hillside seeps. Insets provide the (b) location within Alaska and latitude of the Arctic Circle (dashed line) and (c) synoptic sampling locations within the Salmon River watershed.

evergreen forest (all ≤11.6%) (Dewitz & U.S. Geological Survey, 2021) (Table S3 in Supporting Information S1). The six watersheds encompass a range of lithologies characteristic of the late Mesozoic-Paleogene fold-and thrust belt that forms the northwestern part of the North American Cordillera (Table S4 in Supporting Information S1) (Wilson et al., 2015). Despite this geologic variability, all six watersheds contain geologic units with a high probability of hosting sulfide minerals, including the Hunt Fork Shale and Kayak Shale of the Endicott Group, the Kuna Formation of the Lisburne Group, or chert-bearing units.

Data sets from the Agashashok River and Wulik River were used to evaluate the temporal onset of acid rock drainage. A total of 29 locations in the Agashashok River watershed were surveyed during 2015–2024. Publicly available data from Clawson (2025) were used for the Wulik River watershed, which is located outside the western border of Noatak National Preserve. The watershed contains Red Dog Mine (68.0698°, −162.8723°), one of the world's largest open-pit zinc (Zn), lead (Pb), and silver (Ag) mines. To minimize potential influences from local anthropogenic disturbances, we used data collected from a monitoring station (Ikalukrok Creek, Station 9; 68.0926°, −162.951°; Figure 1) located upstream of discharge from Red Dog Mine. Aside from Red Dog Mine, there is little past or present surface mining and resource extraction within the study area.

2.2. Sample Collection and Processing

Water samples were collected from June to September (2022–2024). To assess the impact of acid rock drainage inputs on river chemistry across the six watersheds, surface water samples were collected from the mainstem, tributaries, and hillside seeps (recently emerged groundwater upwelling on hillsides) (Figure 1). Unimpacted mainstem samples were collected upgradient of any observable point-source input of acid rock drainage (i.e., a hillside seep or impaired tributary) based on visual (e.g., orange discoloration or staining) or chemical indication (e.g., turbidity, specific conductance, and pH) of acid rock drainage at the time of sampling. Mainstem river or creek samples were collected at several locations downstream of acid rock drainage input(s). Tributary samples were collected upstream of the confluence with the mainstem. Hillside seeps were sampled at the location of groundwater upwelling on hillsides. Within watersheds, the number of unique sites ranged from 7 to 27, resulting in 11–43 discrete samples per watershed (Table S1 in Supporting Information S1).

2576604x, 2026, 6, Downloaded from https://agupubs.onlinelibrary.wiley.com/doi/10.1029/2026AV002407 by Jonathan O'Donnell , Wiley Online Library on [24/09/2026]. See the Terms and Conditions (https://onlinelibrary.wiley.com/terms-and-conditions) on Wiley Online Library for rules of use; OA articles are governed by the applicable Creative Commons License

2576604x, 2026, 6, Downloaded from https://agupubs.onlinelibrary.wiley.com/doi/10.1029/2026AV002407 by Jonathan O'Donnell , Wiley Online Library on [24/09/2026]. See the Terms and Conditions (https://onlinelibrary.wiley.com/terms-and-conditions) on Wiley Online Library for rules of use; OA articles are governed by the applicable Creative Commons License

For representative comparisons of downstream chemistry across all watersheds, a single mainstem site located downstream of acid rock drainage input was selected within each watershed to represent the downstream mainstem chemistry ("downstream mainstem" site classification; selection criteria outlined in Section 2.4). The Salmon River, which had the lowest upstream SO_4^{2-} concentration, and multiple downstream point-source acid rock drainage inputs, was sampled in a synoptic fashion in 2023 to quantify downstream transport of acid rock drainage constituents.

At the time of water sample collection, discrete in situ measurements of pH, temperature (°C), dissolved oxygen (DO; mg L^{-1} and % saturation), and specific conductance (SpC; μS cm^{-1}) were collected using a YSI ProDSS multiparameter meter (YSI, Yellow Springs, OH). Sensors were calibrated via manufacturer specifications. Grab samples were collected in a well-mixed area of the mainstems and tributaries using 2-L polyethylene terephthalate glycol (PETG) bottles that were triple rinsed with site water before sample collection and filled with no headspace. Samples at hillside seeps were pumped into 2 L PETG bottles using a Geotech II peristaltic pump (Geotech Environmental, Denver, CO) and acid-cleaned silicone pump tubing. Grab samples were processed on-site at the time of sample collection for all samples from impaired waters or within 24 hr of collection for unimpaired waters. Samples were processed by collecting (a) unfiltered subsamples for quantification of DIC, acid-neutralizing capacity, and unfiltered metals (total major and trace element concentrations) and (b) filtered subsamples (0.45-μm; referred to as filter-passing) for quantification of DOC, dissolved inorganic anions, major cations, trace elements, iron oxidation state (Fe(II) and Fe(III)), and total filter-passing mercury (Hg). Preservation and storage of all samples are defined in Text S1.1 in Supporting Information S1. Field processing blanks involved filtering ultrahigh purity water (≥18.2 MΩ cm) in the field and were collected once per field day over the study period.

2.3. Water Analyses

Complete details of water analyses are provided in Text S1.2, Table S5 in Supporting Information S1. In brief, water samples were analyzed for DIC by acidification and purging, acid-neutralizing capacity by titration to pH 4.5, DOC by high temperature catalytic combustion, major anions (chloride (Cl^-), SO_4^{2-}, nitrate (NO_3^-)) by ion chromatography, major cations (calcium (Ca^{2+}), magnesium (Mg^{2+}), sodium (Na^+) and potassium (K^+)) by Inductively Coupled Plasma-Optical Emission Spectrometry (U.S. EPA, 1994) and major and trace elements (^{9}Be, ^{27}Al, ^{52}Cr, ^{55}Mn, ^{57}Fe, ^{59}Co, ^{60}Ni, ^{63}Cu, ^{66}Zn, ^{75}As, ^{77}Se, ^{89}Y, ^{107}Ag, ^{111}Cd, ^{137}Ba, ^{139}La, ^{140}Ce, ^{141}Pr, ^{146}Nd, ^{163}Dy, ^{205}Tl, ^{206}Pb, ^{207}Pb, ^{208}Pb, and ^{238}U) by Inductively Coupled Plasma-Mass Spectrometry (U.S. EPA, 1998, 2007) (commonly referred to as metals) (see Table S6 in Supporting Information S1 for ICP-MS instrument settings), total filter-passing Hg by cold vapor atomic fluorescence spectrometry (U.S. EPA, 2002), and iron oxidation state by Ferrozine colorimetric analysis (To et al., 1999).

2.4. Site Classification

2.4.1. Five Site Classification Groups

To evaluate changes in downstream chemistry across watersheds, sites were assigned to one of five classification groups (Table 1, Figure S1 in Supporting Information S1). Mainstem samples were classified as either upstream (upstream mainstem; $n = 7$) or downstream (downstream mainstem; $n = 6$) of point-source acid rock drainage inputs (either hillside seeps or impaired tributaries) according to hydrologic and spatial watershed characteristics. Hillside seeps (termed seeps) were acid rock drainage inputs, sampled at the point of groundwater upwelling ($n = 5$). Tributaries were classified as either impaired ($n = 10$) or unimpaired (reference tributaries; $n = 18$) according to visual observations during sample collection and reinforced by in situ chemical measurements (e.g., turbidity, SpC, and pH) and analysis of Google Earth Pro imagery (Google, 2024) using coordinates of sampling locations. With these site classification groups, 46 of the 82 total sites were included in the assessment of downstream chemical changes across the six watersheds. The remaining sites either could not be assigned to a classification group or included mainstem sites outside of the designated upstream and downstream comparison reaches and tributaries for which field observations were insufficient to determine impairment status.

For each sampling site within the mainstem river, a cumulative downstream distance (km), relative downstream distance (km), and relative watershed area were determined. Cumulative downstream distances (km) were measured from the most upstream sampling site in each watershed using the Rule Path tool in Google Earth Pro (Google, 2024). Relative downstream distances (km) were measured for downstream mainstem sampling sites as the downstream river distance from the nearest upstream acid rock drainage input using the Rule Path tool in

2576604x, 2026, 6, Downloaded from https://agupubs.onlinelibrary.wiley.com/doi/10.1029/2026AV002407 by Jonathan O'Donnell , Wiley Online Library on [24/09/2026]. See the Terms and Conditions (https://onlinelibrary.wiley.com/terms-and-conditions) on Wiley Online Library for rules of use; OA articles are governed by the applicable Creative Commons License

Table 1
Site Classification Definitions for Grouping of Sites Across the Six Watersheds

Site classification[a]	Definition
Upstream Mainstem (n = 7)	The most upstream samples in each watershed, upstream of any known point-source acid rock drainage input at the time of sampling. Set at a river distance of 0 km for all downstream sites. Used as control, unimpaired mainstem chemistry
Hillside Seep (n = 5)	Hillside seeps sampled at the location of groundwater upwelling present in four of the six watersheds
Impaired Tributary (n = 10)	Tributaries of the mainstem river that exhibited visual indicators or chemical indication of acid rock drainage at the time of sampling (e.g., orange staining, high relative turbidity, and/or SpC, low pH) compared to the upstream location(s)
Unimpaired Tributary (n = 18)	Tributaries that did not exhibit visual or chemical indicators of acid rock drainage at the time of sampling and used as control, reference tributaries
Downstream Mainstem[b] (n = 6)	Mainstem sites located 6.0–32.6 km downstream of impaired inputs with Relative Watershed Areas between 4.0 and 10.6 (Equation 1). Cumulative downstream distances (from the upstream site) range from 20 to 50 km. across the six watersheds

[a]Refer to Table S1 in Supporting Information S1 for details on the number of sites of each type and unique samples across the six watersheds. [b]Refer to Table S7 in Supporting Information S1 for distances and relative watershed area for each watershed.

Google Earth Pro (Google, 2024). Unique watershed perimeters and area were derived for each mainstem site using a mosaic of 5-m resolution digital elevation models. The Relative Watershed Area was determined for each mainstem site using Equation 1.

$$\text{Relative Watershed Area (unitless)} = \frac{\text{Mainstem Site Watershed Area } (\text{km}^2)}{\text{Upstream Mainstem Watershed Area } (\text{km}^2)} \quad (1)$$

For example, a mainstem site with a Relative Watershed Area of 2.0 equates to the watershed area increasing by a factor of two from the upstream mainstem site. The Relative Watershed Area was used as a consistent metric to group downstream mainstem sites across watersheds of differing size and tributary inputs. Sites in the downstream mainstem grouping had a relative watershed area between 4.0 and 10.6, which equated to a downstream distance (from the nearest input of acid rock drainage) of 6.0–32.6 km and a cumulative downstream distance (from the upstream site) of 20.0–50.0 km (Table 1, Table S7 in Supporting Information S1).

2.5. Hydrological Data

Hydrological data of four gaged streams and rivers regional to the Wulik and Agashashok River watersheds were evaluated from 2015 to 2024. To aid the analysis of historical water quality data, daily discharge data were extracted from the U.S. Geological Survey Water Data for the Nation (U.S. Geological Survey, 2025), for site numbers 15564879 (Slate Creek at Coldfoot, AK), 15743850 (Dahl Creek near Kobuk, AK), 15744500 (Kobuk River near Kiana, AK), and 15747000 (Wulik River below Tutak Creek near Kivalina, AK) using the dataRetrieval package (DeCicco et al., 2022) in R (R Core Team, 2025).

2.6. Calculations and Statistical Analyses

Complete details for the calculations and statistical analyses performed in this study are provided in Text S1.3 in Supporting Information S1. In brief, particulate trace and major elements concentrations were calculated as the difference between unfiltered and filter-passing concentrations. Geochemical speciation predictions were performed using SpecE8 software in The Geochemist's Workbench (Community Edition 18.0) to assess the saturation index of minerals in impaired tributaries (n = 14 conditions) and downstream mainstem sites (n = 9 conditions). Left-censored data were substituted with $\sqrt{2}/2$ times the detection limit (Antweiler, 2015). Bicarbonate (HCO_3^-) concentrations were determined from site-specific DIC, pH, and temperature measurements following equations adapted from U.S. Geological Survey Numbered Series (Rounds & Wilde, 2012). For samples for which acid-neutralizing capacity was not measured, acid-neutralizing capacity was calculated from DIC, pH, and temperature (Rounds & Wilde, 2012). Statistical significance (p-value < 0.05) between site classification groups is displayed on figures by compact letter display.

25766044x, 2026, 6, Downloaded from https://agupubs.onlinelibrary.wiley.com/doi/10.1029/2026AV002407 by Jonathan O'Donnell , Wiley Online Library on [24/09/2026]. See the Terms and Conditions (https://onlinelibrary.wiley.com/terms-and-conditions) on Wiley Online Library for rules of use; OA articles are governed by the applicable Creative Commons License

2.6.1. Relative Tributary Concentrations in the Salmon River

To evaluate how tributary inputs contributed to mainstem river chemistry for the Salmon River synoptic data set, analyte concentration ratios were determined as the ratio of the tributary over the mainstem concentration (Equation 2).

$$\text{Tributary/mainstem concentration ratio} = \frac{\text{Tributary concentration}}{\text{Reference mainstem concentration}} \quad (2)$$

For example, a tributary/mainstem concentration ratio of 5 indicates that the analyte concentration in the tributary was five times greater than that measured at the mainstem immediate upgradient of the confluence (sites identified in Table S8 in Supporting Information S1). For consistency in presentation, pH values were converted to hydrogen ion concentrations for calculation of the tributary/mainstem concentration ratio.

3. Results and Discussion

3.1. Chemistry of Rivers Upgradient of Acid Rock Drainage

Rivers and streams sampled upgradient of point-source acid rock drainage inputs (termed "upstream mainstem") established baseline field conditions (pH, DO concentration, SpC) and aqueous chemistry of the six watersheds during sampling periods (Figures 2 and 3, Figures S2 and S3 in Supporting Information S1). Across watersheds, upstream site pH ranged from 7.89 to 8.33 (Figure 2b), DO ranged from 11.5 to 12.8 mg L^{-1} (near 100% saturation) (Figure 2c), and SpC ranged from 228 to 716 µS cm^{-1} (Figure 2a). DOC concentrations were uniformly low across all six watersheds (<2 mgC L^{-1}) (Figure 2d), while SO_4^{2-} concentrations varied almost an order of magnitude from 25 to 220 mg L^{-1} (Figure 2f) and major divalent cation (Ca^{2+} and Mg^{2+}) concentrations spanned from 20 to 91 mg L^{-1} (Figure 2g) and 6–37 mg L^{-1} (Figure 2h), respectively. Acid-neutralizing capacity was relatively uniform (99.5–117 mg$CaCO_3$ L^{-1}) for five of the watersheds (Agashashok River, Salmon River, Anaktok Creek, Nakolikurok Creek, and Tukpahlearik Creek) but lower in the Kugururok River (52 mg$CaCO_3$ L^{-1}) (Figure 2e). Metal concentrations were low, with the sums of filter-passing metals (summation of all 23 metals measured via ICP-MS) at upstream sites ranging from 44 to 410 µg L^{-1} and the sums of particulate metals ranging from 68 to 2050 µg L^{-1} (Figure 3, Figure S3 in Supporting Information S1). Median concentrations of (a) filter-passing and particulate major metals (Fe, Al, and Mn) were <90 µg L^{-1} and (b) filter-passing and particulate trace (As, Cd, Cu, Co, Cr, Ni, Se, Tl, U, Pb, and Zn) and rare earth elements (REE = ∑Ce, Dy, La, Nd, Pr, and Y) were <30 and <5 µg L^{-1}, respectively.

The chemical compositions of upstream mainstem water across the six watersheds are attributed to differences in bedrock geology and permafrost ice content and interpreted independent of point-source acid rock drainage inputs. First, the relatively low measured major and trace element concentrations were consistent with previous surveys of rivers in the Brooks Range (Rember & Trefry, 2004) and markedly lower than rivers with historical mining that contribute point- and non-point-source metal inputs (Todd et al., 2012). Second, major cation and anion concentrations are indicative of background mineral weathering occurring in the upstream reaches, as evaluated by bedrock composition and the proportions of filter-passing ions (Figure S4 in Supporting Information S1). Upstream mainstem waters were either SO_4^{2-} or HCO_3^- dominant, which indicates the weathering of carbonate bedrock and sulfur mineral sources. Importantly, the hierarchy in mainstem river acid-neutralizing capacity across watersheds is explained by the percentage of carbonate bedrock, with the Kugururok River having the lowest carbonate bedrock (18% of watershed) and the other five watersheds having markedly higher carbonate bedrock (40%–44%) (O'Donnell et al., 2016). Furthermore, SO_4^{2-} concentrations of upstream mainstem waters (median SO_4^{2-} concentrations of each watershed follow the order: Tukpahlearik Creek > Anaktok Creek > Nakolikurok Creek > Kugururok River > Agashashok River > Salmon River) were within the range of concentrations of other headwater streams of the Brooks Range (19–454 mg L^{-1}) (Kemeny et al., 2023; Lehn et al., 2017), and are interpreted to represent the degree of background sulfide mineral weathering and potentially evaporite mineral (e.g., gypsum) dissolution (Kemeny et al., 2023; Lehn et al., 2017; Van Stempvoort et al., 2023). Lastly, the uniformly low DOC concentrations across upstream mainstem sites are consistent with watersheds draining ice-poor permafrost (Carey et al., 2025; O'Donnell et al., 2020). Taken together, these baseline water chemistry data provide a foundation for assessing acid-neutralizing capacity for buffering, background SO_4^{2-} concentrations, and background metal concentrations and partitioning between filter-passing

2576604x, 2026, 6, Downloaded from https://agupubs.onlinelibrary.wiley.com/doi/10.1029/2026AV002407 by Jonathan O'Donnell , Wiley Online Library on [24/09/2026]. See the Terms and Conditions (https://onlinelibrary.wiley.com/terms-and-conditions) on Wiley Online Library for rules of use; OA articles are governed by the applicable Creative Commons License

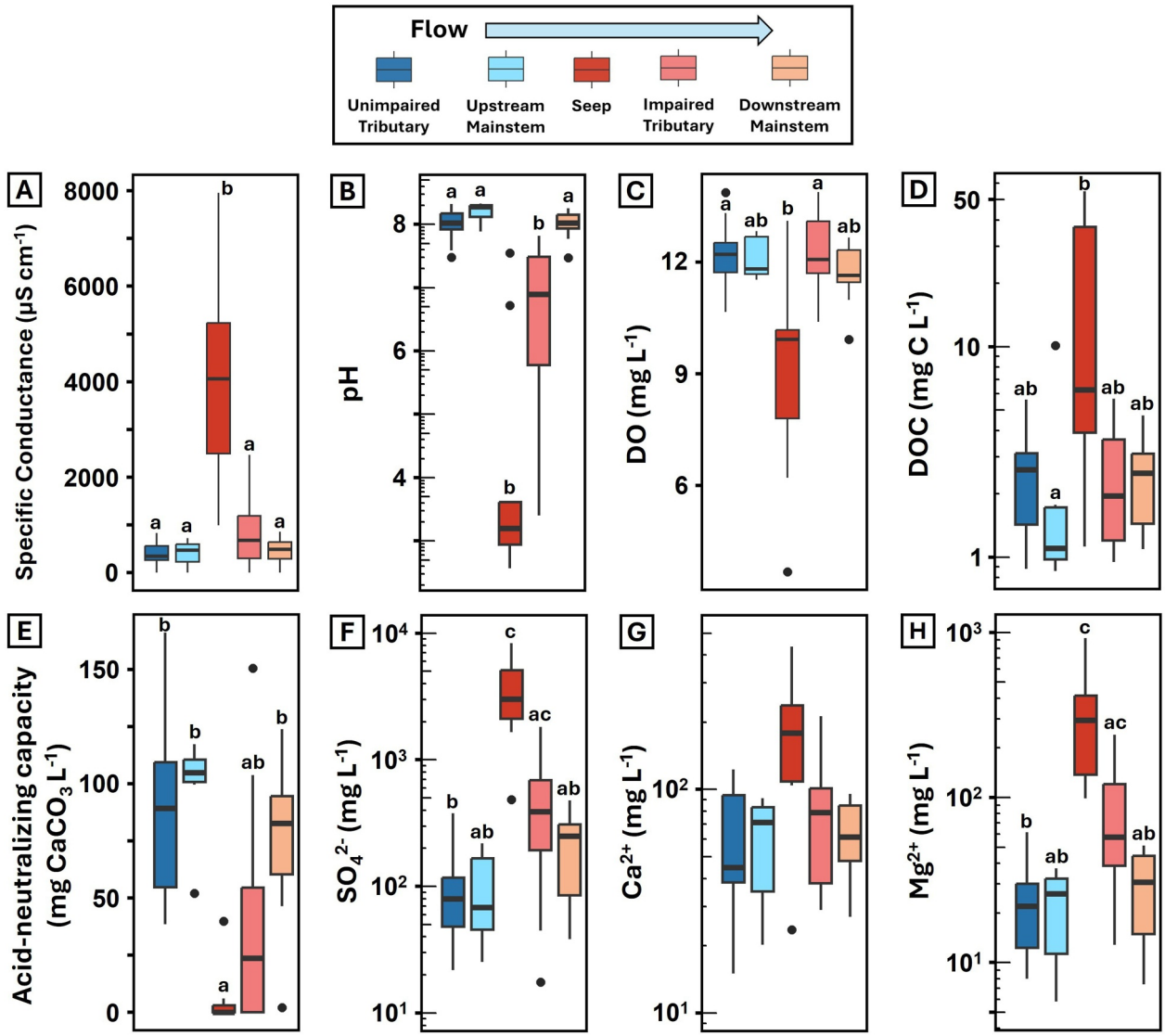


Figure 2. (a) Specific conductance, (b) pH and concentrations of (c) dissolved oxygen, (d) dissolved organic carbon, (e) acid-neutralizing capacity (as $mgCaCO_3\ L^{-1}$), (f) sulfate (SO_4^{2-}), (g) calcium (Ca^{2+}), and (h) magnesium (Mg^{2+}) across the six watersheds by site classification group (Table 1). Boxplots show the median and interquartile range (25th–75th percentiles). Whiskers represent the 10th and 90th percentiles, and observations outside this range are shown as individual points. Statistical significance (p-value < 0.05, Dunn's Test) is displayed by letters (e.g., a–c).

and particulate fractions, which are critical to evaluate the effects of point-source acid rock drainage inputs on downstream chemistry.

3.2. Chemistry of Point-Source Acid Rock Drainage Inputs

Hillside seeps (n = 9) illustrated the distinct geochemical composition of point sources of acid rock drainage across the six watersheds. Seeps were substantially more acidic (pH 2.57–7.55) (Figure 2b), had lower DO concentrations and percent saturation (3.7–13.1 mg L^{-1} and 27.7%–95.9%, respectively) (Figure 2c), higher SpC (991–7,961 µS cm^{-1}) (Figure 2a), lower acid-neutralizing capacity (0.14–39.8 $mgCaCO_3\ L^{-1}$; Figure 2e), and exhibited distinct major and trace element chemistry compared to upstream mainstem waters (Figure 3, Figure S3 in Supporting Information S1). For 34 of the 46 analytes quantified, seeps exhibited higher median concentrations than the upstream mainstem site classification (19 of the 34 statistically significant, Kruskal-Wallis; $p < 0.05$) (Table S9 in Supporting Information S1). The median SO_4^{2-} concentration of seeps was 3,025 mg L^{-1} (and as high as 8,300 mg L^{-1}), which was 44 times greater than the median of upstream mainstem waters (Kruskal-

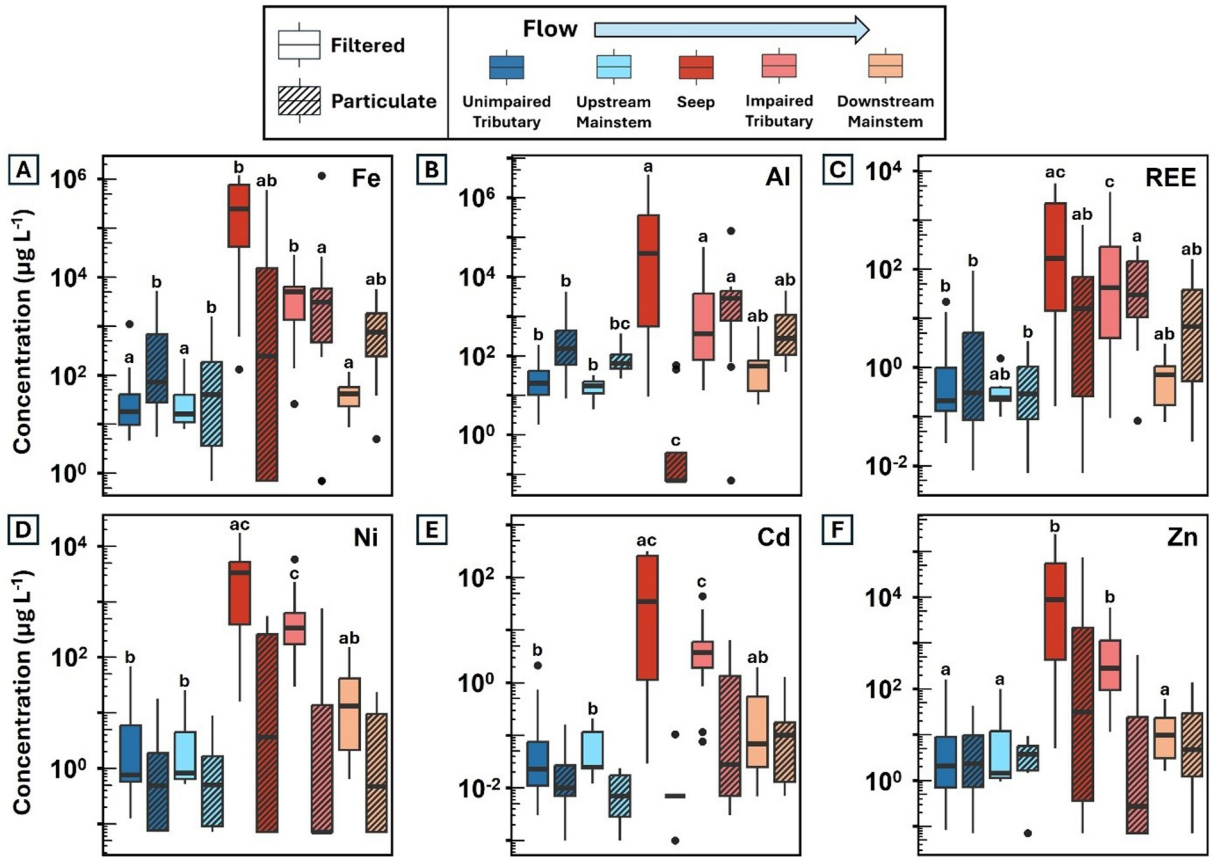


Figure 3. Concentrations of filter-passing and particulate (a) iron (Fe), (b) aluminum (Al), (c) summation of rare earth elements (REE; ∑Ce, Dy, La, Nd, Pr, and Y), (d) nickel (Ni), (e) cadmium (Cd), and (f) zinc (Zn) across the six watersheds by site classification group (Table 1). Boxplots show the median and interquartile range (25th–75th percentiles). Whiskers represent the 10th and 90th percentiles, and observations outside this range are shown as individual points. Statistical significance (p-value < 0.05, Dunn's Test) is displayed by letters (e.g., a–c) independently between filter-passing and particulate data between classification groups.

Wallis; $p < 0.05$; Figure 2f). Further, DOC and Mg^{2+} concentrations were significantly higher in seeps (1.1–55 mgC L^{-1} and 99–922 mg L^{-1}, respectively; Kruskal–Wallis; $p < 0.05$) (Figures 2d and 2h) than upstream mainstem waters. In seeps, metals were present primarily in the filter-passing fraction (average ~ 97% of total metal) with filter-passing concentrations of Fe, Mn, Al, REE, Ni, Cd, and Zn 2.9–4.2 orders of magnitude greater than the upstream mainstem waters (Kruskal–Wallis; $p < 0.05$; Figure 3, Figure S3 in Supporting Information S1). Filter-passing concentrations of Co and Cu in seeps were comparatively lower (median concentrations of 80 and 605 µg L^{-1}, respectively) but still elevated in seeps relative to upstream mainstem waters (Figure S3 in Supporting Information S1; Kruskal Wallis; $p < 0.05$). Importantly, Pb, As, and Hg concentrations were relatively low in seeps (<10 µg L^{-1} for Pb and As; <4 ng L^{-1} for Hg) (Figures S3f and S3h in Supporting Information S1).

An assessment of the pH and metal concentrations of seeps revealed high potential for acid generation and metal release across the watersheds (Figure 4a). Seeps in the Agashashok River, Tukpahlearik Creek, and Anaktok Creek watersheds were highly acidic and metal-rich (∑Zn + Cu + Cd + Pb + Co + Ni), as defined by classifications used for acid mine drainage (Ficklin et al., 1992; Plumlee, 1997). For regional comparison, these seeps were more acidic (pH < 4) and metal-rich compared to natural acid rock and acid mine drainage waters across the Su-Lik and Red Dog massive sulfide deposits of Alaska's Brooks Range (shown as gray symbols in Figure 4a) (Kelley & Taylor, 1997) and consistent with extreme acid mine drainage conditions. One seep in the Nakolikurok Creek watershed had a higher pH and lower filter-passing metal concentrations and was characterized as "near-neutral/low-metal" water, with metal concentrations comparable to those observed in the upstream sites of our study (refer to the blue shaded region in Figure 4a). Notwithstanding, the low pH and extremely high metal concentration of seeps observed across watersheds demonstrate the extreme potential for acid generation and metal release across watersheds spanning the western Brooks Range.

2576604x, 2026, 6, Downloaded from https://agupubs.onlinelibrary.wiley.com/doi/10.1029/2026AV002407 by Jonathan O'Donnell , Wiley Online Library on [24/09/2026]. See the Terms and Conditions (https://onlinelibrary.wiley.com/terms-and-conditions) on Wiley Online Library for rules of use; OA articles are governed by the applicable Creative Commons License

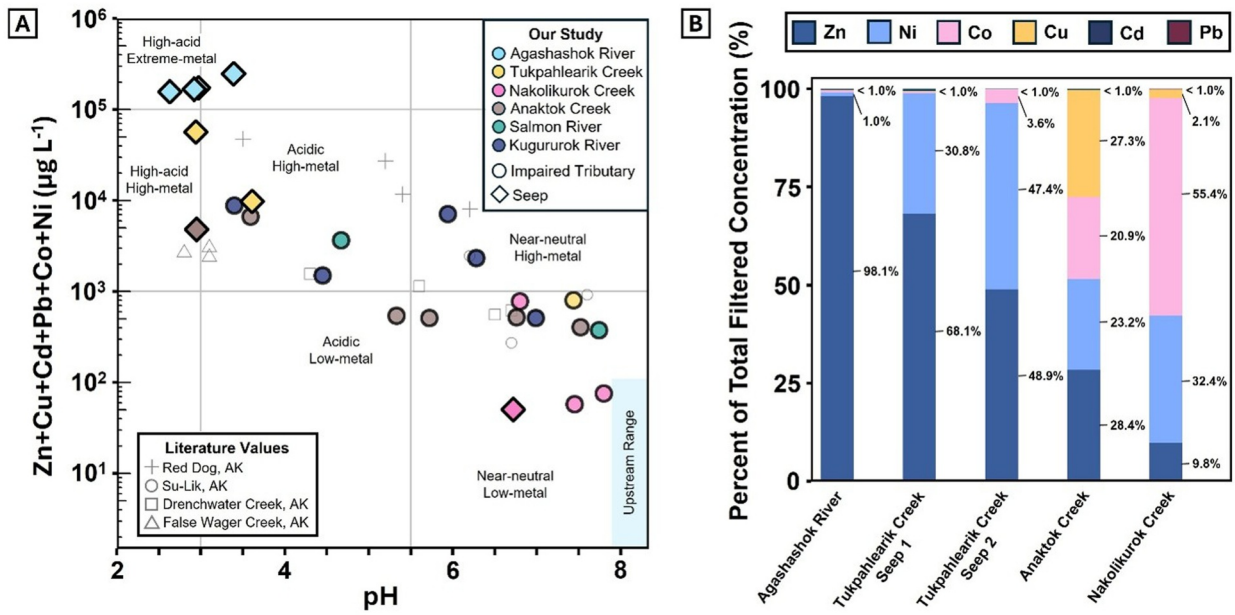


Figure 4. (a) Metal concentrations of seeps (diamonds) and impaired tributaries (circles) versus field-measured pH by watershed, in context of acid and metal conditions of acid mine drainage (defined by Plumlee, 1997) and previous literature values (Graham & Kelley, 2009; Kelley & Taylor, 1997). (b) Relative proportion of filter-passing metal concentrations (as a percentage of ∑Zn, Ni, Cu, Co, Cd, and Pb) of seep samples.

The geochemical data of seeps, including low pH, DO concentrations markedly lower than saturation (Elberling, 2005), and elevated SO_4^{2-} and major and trace element concentrations (Figures 2 and 3), are consistent with sulfide mineral oxidation as the dominant underlying mechanism driving metal release (Alpers et al., 2003; Graham & Kelley, 2009; Nordstrom & Alpers, 1999). Further, the distribution of Fe oxidation state was measured within the acidic Agashashok River seep ($2.9 \leq pH \leq 3.4$) and showed the co-presence of Fe(II) and Fe(III) (72% and 28%, respectively) (Table S10 in Supporting Information S1). This observation suggests the potential for microbial oxidation of Fe(II) to Fe(III) in the subsurface, the latter further catalyzing sulfide mineral oxidation (Kirby et al., 1999; Nordstrom, 2000), and may help explain the low pH of the majority of the seeps at which the rate of abiotic oxidation of Fe(II) to Fe(III) is significantly reduced (Kirby et al., 1999; Nordstrom, 2011). However, given the lack of access to the host sulfide minerals and subsurface hydrological flow paths, and unknown microbial community composition, we cannot quantitatively account for buffering or differences in the extent of coupled abiotic/biotic processes that accelerate sulfide mineral oxidation that may have occurred in the subsurface (Nordstrom, 2000; Schippers & Sand, 1999).

The distributions of metals across seeps differed markedly between and within watersheds (Figure 4b), particularly in the relative abundance of Zn, Ni, Co, and Cu. We interpret this as indicating the different source minerals being weathered (e.g., pyrite and base-metal sulfides). For example, the Agashashok River seep may indicate the weathering of sphalerite (ZnS), which would contribute to the higher proportion of Zn observed, whereas Cu-rich sulfide minerals or impurities (covellite (CuS) or chalcopyrite ($CuFeS_2$)) may explain the highest proportion of Cu across seep chemistry in the Anaktok Creek watershed (Figure 4b). The diverse composition of seep metal chemistry and potential source minerals is consistent with the known variety of sulfide deposits (Kelley & Jennings, 2004; Schmidt, 1997) and sulfide-bearing geologic units across the six watersheds (Table S4 in Supporting Information S1) (Wilson et al., 2015).

Impaired tributaries ($n = 21$) were more acidic (pH range of 3.40–7.82) and had higher metal (sum of filter-passing metals ranged from 522 to 130,900 µg L^{-1}, and sum of particulate metals ranged from 382 to 1,329,200 µg L^{-1}) and SO_4^{2-} concentrations (17.6–1,820 mg L^{-1}) than upstream or reference tributary groups (Figures 2 and 3, Figures S2 and S3 in Supporting Information S1; no statistical difference to seeps using Kruskal-Wallis test, $p > 0.05$). Impaired tributaries showed highly consistent trends between pH and metal concentration (Figure 4a) but contained a greater proportion of metals in the particulate fraction (on average ~20% particulate of total metals) than seeps, whereas seeps contained metals predominantly in the filter-passing fraction (on average

2576604x, 2026, 6, Downloaded from https://agupubs.onlinelibrary.wiley.com/doi/10.1029/2026AV002407 by Jonathan O'Donnell , Wiley Online Library on [24/09/2026]. See the Terms and Conditions (https://onlinelibrary.wiley.com/terms-and-conditions) on Wiley Online Library for rules of use; OA articles are governed by the applicable Creative Commons License

2576604x, 2026, 6, Downloaded from https://agupubs.onlinelibrary.wiley.com/doi/10.1029/2026AV002407 by Jonathan O'Donnell , Wiley Online Library on [24/09/2026]. See the Terms and Conditions (https://onlinelibrary.wiley.com/terms-and-conditions) on Wiley Online Library for rules of use; OA articles are governed by the applicable Creative Commons License

~3% particulate) (Figures S5 and S6a in Supporting Information S1). This was most evident for Al, As, Cr, Pb, REE, Se, and U which were disproportionately high in the particulate fraction compared to filter-passing fraction in the impaired tributaries, whereas Ba, Cd, Co, Cu, Mn, Ni, and Zn were predominantly in the filter-passing fraction (Figure S6b in Supporting Information S1). Geochemical modeling of impaired tributary conditions (described in Text S1.4 in Supporting Information S1) assessed whether tributaries were undersaturated or supersaturated with respect to mineral phases. At the field conditions of impaired tributaries (e.g., pH, DO concentration, temperature, acid-neutralizing capacity concentration, filter-passing major cation, anion and metal concentrations), several minerals were supersaturated ($Q > K$) including Fe and Mn (oxy)hydroxides (e.g., Fe$(OH)_3$ and MnO(OH)), mixed metal-substituted Fe oxides (e.g., $Co(FeO_2)_2$, $NiFe_2O_4$, $CuFe_2O_4$, and $ZnFe_2O_4$), and Fe(III) sulfate and Al(III) sulfate minerals ($(Na,K)Fe_3(SO_4)_2(OH)_6$ and $KAl_3(SO_4)_2(OH)_6$) (Table S11 in Supporting Information S1). Therefore, the chemistry of impaired tributaries is interpreted to be driven by acidic seep inputs within the watershed and a combination of dilution, mineral precipitation, and metal adsorption to the surfaces of Fe(III) and Mn(III) oxide and (oxy)hydroxide, resulting in greater particulate metal concentrations at higher pH (Gault et al., 2015).

We interpret the acidic water, metal concentration (Figures 3 and 4a, Figure S3 in Supporting Information S1), and distribution of metals (Figure 4b) in seeps and impaired tributaries to represent the source materials of weathered minerals (e.g., pyrite and base-metal sulfides), extent of sulfide mineral oxidation reactions, potential subsurface buffering by acid-neutralizing minerals (e.g., carbonates) across the watersheds (Graham & Kelley, 2009; Plumlee, 1997), and dilution and mineral precipitation. Although we observed watershed-specific differences in metal concentration and fraction distribution (filter-passing vs. particulate) across seeps and impaired tributaries, the chemistry of seeps and impaired tributaries was distinct from upstream mainstem and unimpaired tributary sites (Figure 3 and Figure S3 in Supporting Information S1) highlighting the potential for their input to affect mainstem river chemistry.

3.3. Downstream Effects of Acid Rock Drainage Inputs

3.3.1. Effects of Acid Rock Drainage Chemistry Across Six Watersheds

We examined the downstream fate of the constituents from point-source acid rock drainage inputs across all watersheds by comparing the chemistry of the downstream mainstem group (encompassing sites 6.0–32.6 km downstream of upstream sites) to the chemistry of the upstream group (Figures 2 and 3, Figures S2 and S3 in Supporting Information S1). Compared to the upstream group, downstream mainstem pH had a slightly greater range (pH of 7.47–8.25) but was not substantially different from the upstream group (7.89–8.33). However, 31 of 45 analytes measured had higher downstream median concentrations compared to the upstream group, 7 of which were statistically significant (Kruskal–Wallis; $p < 0.05$). Notably, the median SO_4^{2-} concentration downstream was 182 mg L^{-1} higher than upstream (Figure 2f), with the Salmon River watershed exhibiting a 962% increase (from 25.3 to 269 mg L^{-1}) (Figure S7 in Supporting Information S1). Median acid-neutralizing capacity was lower downstream compared to upstream of acid rock drainage inputs (83 mg$CaCO_3$ L^{-1} vs. 105 mg$CaCO_3$ L^{-1}), interpreted to be from consumption of acid-neutralizing capacity from acidic tributary and seep inputs (Kemeny et al., 2021). Yet, the stable downstream mainstem river pH (Figure 2b) indicates the six watersheds had sufficient acid buffering capacity to prevent mainstem river acidification.

We observed significant differences between upstream and downstream median concentrations of select filter-passing and particulate metals, ranging from 3- to 21-fold increases. Ni concentrations only increased in the filter-passing fraction (0.8–13 μg L^{-1}), Fe and the sum of REE only increased in the particulate fraction (41–756 and 0.3–7 μg L^{-1}, respectively), and Al increased in both the filter-passing and particulate fraction (18–55 and 65–282 μg L^{-1}, respectively) (Figure 3; Kruskal–Wallis; $p < 0.05$). Particulate Ni, Zn, and Cd were comparable between downstream and upstream sites (<1 μg L^{-1}). Filter-passing Mn increased 7-fold (from 13 to 96 μg L^{-1}) between upstream to downstream (Figure S3 in Supporting Information S1), but differences were not statistically significant ($p > 0.05$). Watershed-specific differences were observed in the magnitude of changes in filter-passing and particulate constituent concentrations (Figure S7 in Supporting Information S1) that aligned with the observations across all six watersheds when grouped (Figure 3, Figure S3 in Supporting Information S1). All other filter-passing and particulate elements (As, Co, Cr, Cu, Se, Tl, U, and Pb) were within the same concentration range downstream as upstream of point-source inputs of acid rock drainage (difference within 1.5 μg L^{-1}).

2576604x, 2026, 6, Downloaded from https://agupubs.onlinelibrary.wiley.com/doi/10.1029/2026AV002407 by Jonathan O'Donnell , Wiley Online Library on [24/09/2026]. See the Terms and Conditions (https://onlinelibrary.wiley.com/terms-and-conditions) on Wiley Online Library for rules of use; OA articles are governed by the applicable Creative Commons License

Specific constituents and fractions that remained elevated downstream of acid rock drainage inputs across watersheds align with the chemical characterization of seeps and impaired tributaries, the geochemical susceptibility of constituents to precipitate or absorb to solid phases, and dilution from downstream tributaries. Unimpaired tributaries between the upstream and downstream mainstem sites universally showed similar chemistry to upstream sites (Figures 2 and 3; Figures S2 and S3 in Supporting Information S1), therefore diluting acid rock drainage inputs as the watershed area increased in size from upstream to downstream sites (from 6- to 10.4-fold). This, in part, explains why many analytes were only modestly higher downstream when data were grouped across all six watersheds, with markedly increased SO_4^{2-} and select filter-passing (Al, Ni, Mn) and particulate metal concentrations (Fe, Al, and REE). Geochemical modeling (Text 1.4 in Supporting Information S1) of the downstream water chemistry shows that most waters were supersaturated with respect to Fe(III) minerals (Table S12 in Supporting Information S1) consistent with elevated particulate Fe (Figure 3a), and thus Fe(III) minerals are expected to preferentially adsorb select metals (e.g., Co and Cu and REE) (Gault et al., 2015) with minimal adsorption of Ni. Although thermodynamic modeling also predicted precipitation of Mn minerals, Mn remained elevated in the filter-passing fraction across downstream mainstem sites (Figure S3A in Supporting Information S1) likely due to relatively slow abiotic oxidation of Mn(II) by DO (Hem, 1963; Morgan & Lahav, 2007); therefore, Mn(IV) minerals were not considered a major contributor to adsorption of other metals. For As and Pb, acid rock drainage inputs had no effect on mainstem river concentrations because of their low concentrations (<10 μg L^{-1}) in seeps and impaired tributaries (Figures S3f and S3h in Supporting Information S1).

Conversely, SO_4^{2-} was not expected to adsorb to minerals downstream in the mainstem rivers due to the relatively high pH (pH range of 7.47–8.25; Munk et al., 2002) nor was SO_4^{2-} mineral precipitation in the mainstem rivers expected at these distances downstream (6.0–32 km downstream of acid rock drainage inputs) based on geochemical modeling of the downstream mainstem sites. $BaSO_4$ was the only sulfate mineral slightly supersaturated but the formation would be limited by the low concentrations of Ba^{2+} ($\leq$24 μg L^{-1}) relative to SO_4^{2-} ($>$251 mg L^{-1}) (Table S12 in Supporting Information S1). The formation of Fe(III) and Al(III) secondary sulfate minerals is only expected within impaired tributaries (Table S11 in Supporting Information S1), consistent with previous observed (Lacelle et al., 2007; Nordstrom, 2000; Skierszkan et al., 2026), but not the mainstem rivers. Therefore, the pronounced enrichment of SO_4^{2-} observed across watersheds (Figure 2f), in conjunction with thermodynamic modeling results (Table S12 in Supporting Information S1), indicates that SO_4^{2-} is a viable proxy for acid rock drainage inputs to rivers.

In summary, when data were grouped across watersheds, the results provide evidence of a downstream effect on water chemistry at mainstem sites located 6.0–32.6 km downstream of acid rock drainage inputs, including elevated concentrations of filter-passing SO_4^{2-}, filter-passing Al, Ni, and Mn, and particulate Fe, Al, and REE. These results indicated that downstream effects within our study area are driven by the acidity, metal concentration, and metal fraction distribution contributed by seeps and impaired tributaries. To build on these observations across watersheds, a spatially resolved analysis was conducted within a single watershed to investigate transport chemistry and transport distances.

3.3.2. Salmon River Synoptic Analysis of Downstream Fate

A spatially resolved analysis of the downstream fate of acid rock drainage inputs was conducted across 19 sites in the Salmon River watershed spanning 103 km (Figure 1c). The Salmon River watershed was well suited for this evaluation because the upstream site had the highest pH (8.33) and lowest SO_4^{2-} concentration (25 mg L^{-1}) of the six watersheds, and relatively low filter-passing and particulate metal concentrations (sum of filter-passing metals = 43 μg L^{-1}; sum of particulate metals = 174 μg L^{-1}). Trends in analyte concentrations were evaluated over 103 km of the mainstem of the Salmon River from the upstream site to downstream site as a function of the relative watershed area (from 1 to 22.3; Equation 1) (Figure 5), over which nine tributaries enter ($n = 5$ acid rock drainage impaired tributaries; $n = 4$ unimpaired tributaries). Tributary chemistries were evaluated relative to mainstem chemistry and are presented as a tributary/mainstem concentration ratio (Equation 2) in heat plots.

Mainstem river pH and SO_4^{2-} concentration exhibited abrupt shifts that persisted downstream. The first and second impaired tributaries entered at a relative watershed area of 3.75 and 4.75 (pH 7.74 and 4.67, respectively), resulting in a decrease in mainstem river pH from 8.33 to 7.71, followed by a rebound from 7.71 to ∼8.0 and remained consistent as the watershed area increased to the final downstream site (Figure 5a). Mainstem river SO_4^{2-} concentration showed a step-increase at the locations of the two uppermost impaired inputs (with SO_4^{2-}

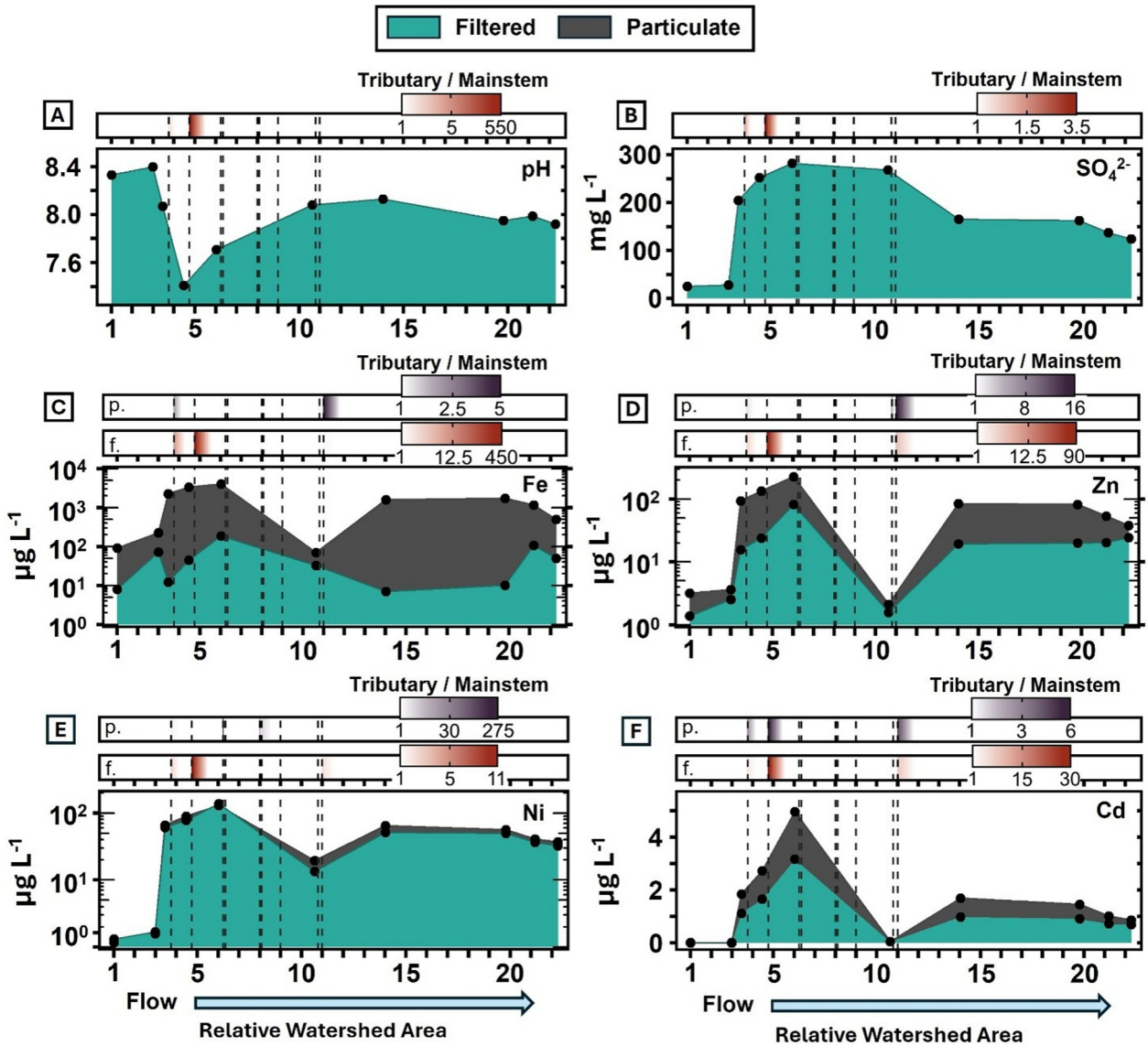


Figure 5. Spatial analysis of the Salmon River mainstem and tributary (a) pH and concentrations of (b) sulfate (SO_4^{2-}) and particulate (p.) and filter-passing (f.) (c) iron (Fe), (d) zinc (Zn), (e) nickel (Ni), and (f) cadmium (Cd) from upstream to downstream presented as the Relative Watershed Area (Equation 1). Area plots show the mainstem river concentrations at discrete mainstem sampling locations indicated by the black symbols. The hashed vertical lines identify locations of tributaries according to their distance downstream. Heat plots above each sub-plot present the tributary versus mainstem concentration ratio (Equation 2), where color saturation indicates the analyte concentration ratio with unique legends for each analyte.

concentrations of 407 and 880 mg L^{-1}, respectively), increasing from 25 mg L^{-1} upstream to a maximum concentration of 280 mg L^{-1} (Figure 5b). Then, SO_4^{2-} concentration progressively decreased to 124 mg L^{-1} at the furthest downstream site, exhibiting a total increase of ~100 mg L^{-1} from upstream to downstream.

Particulate and filter-passing metals (Fe, Zn, Ni, and Cd) show three zones of concentration changes across the mainstem. These metals concentrations increased from impaired tributary inputs located at relative watershed area values of 4.75 and 11.0 and decreased across the intervening reach at relative watershed areas of 6.0–10.0 (Figures 5c–5f). Enrichment of Fe was primarily observed in the particulate fraction, with a ~30-fold increase observed in the mainstem after the impaired tributary input at relative watershed area of 11.0 (Figure 5c). Zn and Cd exhibited enrichment in both filter-passing and particulate fractions, with the most pronounced increases associated with impaired tributary inputs at a relative watershed area of 4.75 (up to 260-fold increase) and 11.0 (up to 120-fold) (Figures 5d and 5f). In total, filter-passing and particulate Zn increased 17.6 and 7.7-fold (from

2576604x, 2026, 6, Downloaded from https://agupubs.onlinelibrary.wiley.com/doi/10.1029/2026AV002407 by Jonathan O'Donnell , Wiley Online Library on [24/09/2026]. See the Terms and Conditions (https://onlinelibrary.wiley.com/terms-and-conditions) on Wiley Online Library for rules of use; OA articles are governed by the applicable Creative Commons License

2576604x, 2026, 6, Downloaded from https://agupubs.onlinelibrary.wiley.com/doi/10.1029/2026AV002407 by Jonathan O'Donnell , Wiley Online Library on [24/09/2026]. See the Terms and Conditions (https://onlinelibrary.wiley.com/terms-and-conditions) on Wiley Online Library for rules of use; OA articles are governed by the applicable Creative Commons License

1.4 to 24 and 1.8–14 μg L^{-1}, respectively), and filter-passing and particulate Cd increased 28.2 and 22.8-fold (from 0.03 to 0.71 μg L^{-1} and <DL to 0.16 μg L^{-1}, respectively). Conversely, Ni concentrations increased primarily in the filter-passing fraction by nearly two orders of magnitude (from 0.5 to 32.4 μg L^{-1}) that persisted across the 103 km (Figure 5e). Similar dynamics were observed for other major and trace elements (Figure S8 in Supporting Information S1), with Cu, REE, and Se showing enrichment primarily in the particulate fraction, Al showing enrichment of both filter-passing and particulate fractions, and Mn and Co showing enrichment primarily as filter-passing fraction.

Trends in filter-passing and particulate analyte concentrations were a function of the locations of the impaired tributary inputs (relative watershed area values of 3.75, 4.75, and 11.0), the concentration and fraction in which each constituent was delivered (filter-passing vs. particulate), susceptibility to precipitation and/or adsorption, and dilution effects by unimpaired tributary inflows (between relative watershed area values of 6 and 10) and potential groundwater inputs. SO_4^{2-}, expected to behave nearest to a conservative analyte, exhibited the greatest relative increase across the 103 km. Impaired tributaries contributed particulate and filter-passing Fe, Zn, and Cd and filter-passing Ni, with demonstrated effects on filter-passing (Fe, Zn, Ni, and Cd) and particulate metal concentrations (Fe, Zn, and Cd), highlighting the potential for long range downstream transport. The continuum of preferential adsorption observed in other acid drainage systems (Cu > Zn > Ni > Cd; Baleeiro et al., 2018; Munk et al., 2002), including REEs (Bau, 1999; Verplanck et al., 2004), that increases at higher pH, is largely consistent with the observed with the fraction distribution and persistence of Ni, Zn, and Cd in the Salmon River.

The observations of downstream transport of acid rock drainage constituents in the Salmon River watershed are largely consistent with observations across all six watersheds (Figure 3, Figure S3 in Supporting Information S1), yet the magnitude of downstream increases in constituent concentrations was much greater in the Salmon River (Figure 5). The susceptibility of a river to effects of acid rock drainage is a product of (a) the quantity, chemical composition, and relative discharge of impaired inputs (seeps and impaired tributaries), (b) mainstem dilution from unimpaired tributaries, and (c) metal adsorption and particle sedimentation. Further, non-point sources of acid rock drainage (e.g., via subsurface groundwater flow), recognized as important inputs in acid mine drainage systems (Kimball et al., 2002), and buffering of acidic sources from in-stream mineral buffering from carbonates or acid neutralizing tributary and groundwater inputs (Skierszkan et al., 2026), may have contributed to our observations here.

3.4. Temporal Onset of Acid Rock Drainage

Our evaluation of the downstream effects of acid rock drainage inputs across six watersheds provide critical spatial information but was temporally limited to the summers of 2022 and 2023. However, up to 200 rivers and streams across the Brooks Range have developed evidence of acid rock drainage in the recent past (O'Donnell et al., 2024, 2025; Sullivan et al., 2025). Here, we use geochemical indicators (SO_4^{2-}, total Zn, acid-neutralizing capacity) to evaluate the temporal dynamics of acid rock drainage (i.e., onset and recovery) in two watersheds in our study area. The Agashashok River watershed (O'Donnell et al., 2024) has a known point-source of acid rock drainage (hillside seep, 67.585°, −161.816°) that, based on remotely sensed images, emerged during the summer of 2019 (O'Donnell et al., 2024). We further evaluated temporal data of the Wulik River (Figure 1; Station 9) upstream of where treated water from the Red Dog Mine is discharged into the mainstem (refer to Section 2.1 for additional details).

Using SO_4^{2-} concentration as a geochemical tracer of acid rock drainage, mainstem river chemistry on the Agashashok River was evaluated for 2015–2024 (Figure 6) and categorized into early summer (May–June) and late summer (August–September) to differentiate periods with shallow and deep active thaw thicknesses, respectively. Pre-onset SO_4^{2-} concentrations were 17.7 ± 12.7 mg/L (mean ± standard deviation; $n = 46$) in early season and 32.1 ± 17.9 mg/L ($n = 68$) in late season. Post-onset concentrations of SO_4^{2-} were significantly greater than pre-onset in both early and late season, representing 174% and 224% increases, respectively (Wilcoxon, $p < 0.05$; Figure 6a). The highest SO_4^{2-} concentrations were observed in late summer 2019, during the first sampling after visual identification of the seep (O'Donnell et al., 2024). In the Wulik River from 2015 to 2024, post-onset SO_4^{2-} concentrations in both early and late season (Table S13 in Supporting Information S1) represented significant 263% and 197% increases, respectively (Wilcoxon, $p < 0.05$; Figure 6b) relative to pre-onset concentrations. SO_4^{2-} concentrations were greatest in 2020, followed by a systematic decrease from 2020

10.1029/2026AV002407

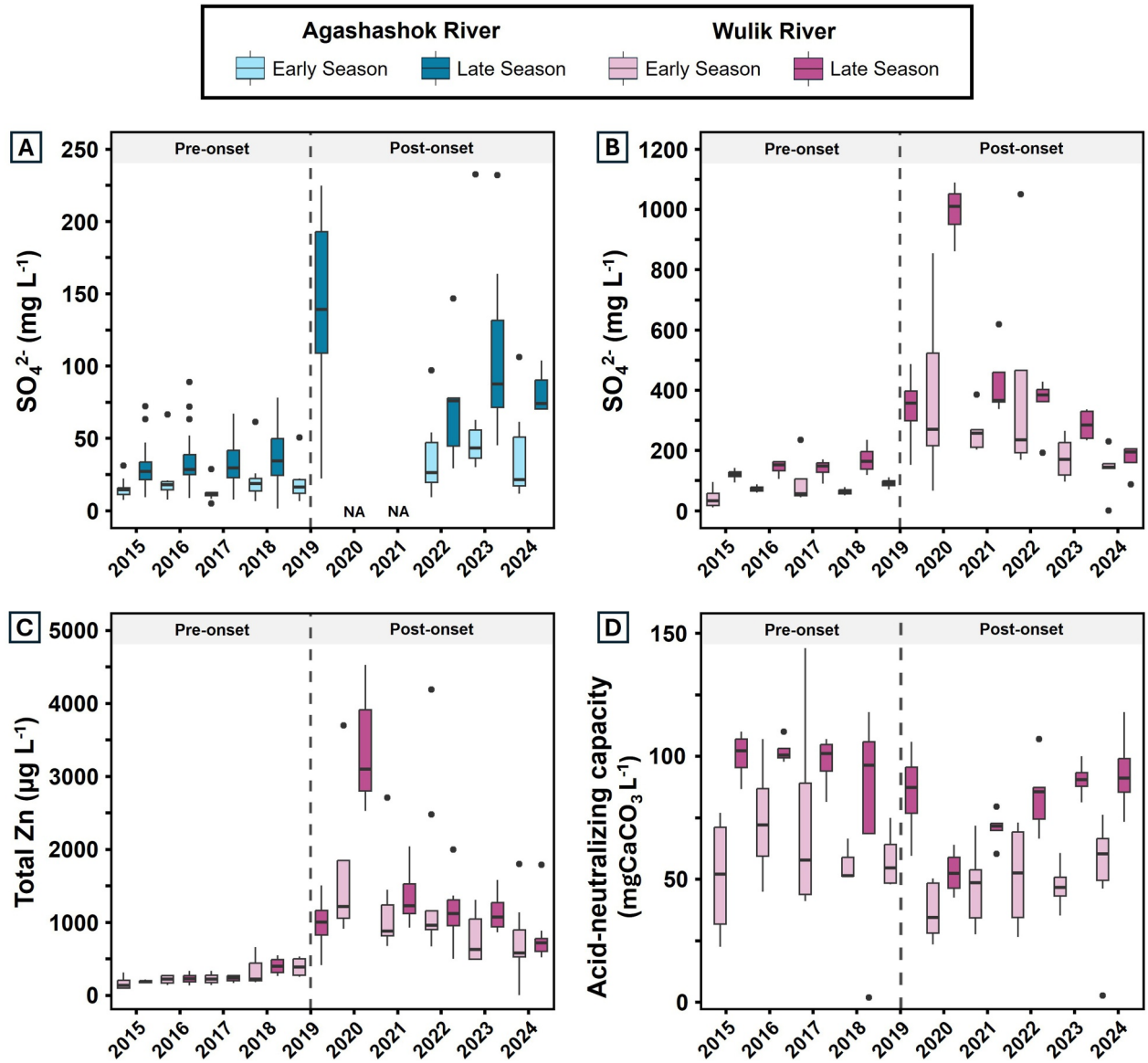


Figure 6. Temporal evaluation of (a) the Agashashok River mainstem and tributary concentrations of sulfate (SO_4^{2-}) and (b) the Wulik River (Station 9, Ikalukrok Creek) SO_4^{2-}, (c) total zinc (Zn), and (d) acid-neutralizing capacity (as mg$CaCO_3$ L^{-1}) during 2015–2024. Boxplots present median and quartile ranges for early season (May–June) and late season (August–September) periods. Dashed vertical lines indicate the visual onset of the seep flow in Agashashok River (O'Donnell et al., 2024). In 2020 and 2021, samples were not collected in the Agashashok River. One measurement in subplot C in 2024 early season was excluded because it was below detection limit (<0.006 µg L^{-1}), and two measurements in subplot C in late season 2023 and early season 2024 were excluded (>10,000 µg L^{-1}).

through 2024 indicating a period of recovery within the watershed. The timing and step increases in SO_4^{2-} concentration were consistent across both watersheds.

Further, total Zn concentration data (filter-passing plus particulate Zn) from the Wulik River showed significant increases by up to 770% between pre- and post-onset periods (Table S13 in Supporting Information S1) (Wilcoxon, $p < 0.05$; Figure 6c). Similar to SO_4^{2-} in the Wulik River, total Zn showed a step-increase in 2019–2020 and then decreased from 2021 to 2024 (Figure 6c). As our findings from this study document, other metals are expected to be elevated in acid rock drainage (Ni, Fe, Al, Cd, REE; Figures 3 and 5, Figure S3 in Supporting Information S1) but were not evaluated. Fluctuations in acid-neutralizing capacity were also observed to be concurrent with observed increases and decreases in SO_4^{2-} and total Zn concentrations (Figure 6d), where years with the greatest SO_4^{2-} and total Zn concentrations had the lowest acid-neutralizing capacity concentrations

2576604x, 2026, 6, Downloaded from https://agupubs.onlinelibrary.wiley.com/doi/10.1029/2026AV002407 by Jonathan O'Donnell , Wiley Online Library on [24/09/2026]. See the Terms and Conditions (https://onlinelibrary.wiley.com/terms-and-conditions) on Wiley Online Library for rules of use; OA articles are governed by the applicable Creative Commons License

2576604x, 2026, 6, Downloaded from https://agupubs.onlinelibrary.wiley.com/doi/10.1029/2026AV002407 by Jonathan O'Donnell , Wiley Online Library on [24/09/2026]. See the Terms and Conditions (https://onlinelibrary.wiley.com/terms-and-conditions) on Wiley Online Library for rules of use; OA articles are governed by the applicable Creative Commons License

(2019 and 2020). This pattern was interpreted to indicate the consumption of acid buffering capacity during these periods of increased acid rock drainage inputs in 2019 and 2020 (Sherlock et al., 1995; Short et al., 1990).

Interannual fluctuations in discharge, which can affect analyte concentration, were considered over this period (2015–2024) from four nearby hydrologic stations to assess if analyte concentrations could be influenced by dilution (Manning et al., 2024; Skierszkan et al., 2026; Zarroca et al., 2021). Across all four stations, the cumulative annual discharge showed modest increases during 2015–2024, with cumulative discharge during the late season in 2019 and 2020 being comparable to previous years discharge during the same months (Figure S9 in Supporting Information S1). The stations had statistically higher average cumulative yearly discharge in post-onset years (2019–2024) relative to pre-onset (2015–2018) for both early and late season for all stations, excluding early season at the Wulik River station (Wilcoxon, $p < 0.05$; Figure S10 in Supporting Information S1). Greater cumulative yearly discharge between pre- and post-onset years would be expected to dilute SO_4^{2-} and metal concentrations, which is the opposite of the observed step-increases (Figure 6). Further, changes in Cl^- concentration (and the ratio of SO_4^{2-}:Cl^-) in the Wulik and Agashashok River watersheds were evaluated, because Cl^- concentration is independent of sulfide mineral oxidation. Between 2015 and 2024, Cl^- concentrations exhibited a minimal decrease (Figures S11c and S11d in Supporting Information S1) and the SO_4^{2-}:Cl^- ratio increased (Figures S11e and S11f in Supporting Information S1), indicating increased SO_4^{2-} concentration in post-onset years (Figure 6). Therefore, we conclude that step-increases in SO_4^{2-} and total Zn concentrations were independent of interannual variability in hydrology and rather indicate increases of acid rock drainage in the watersheds, which is consistent with observed acid rock drainage onset within the Yukon River and Mackenzie River basins in Canada (Skierszkan et al., 2026).

The onset timing of increased acid rock drainage in both watersheds (2019–2020) is consistent with remote sensing observations of orange staining in multiple watersheds (Salmon River, Kugururok River, and Anaktok Creek) (O'Donnell et al., 2024). Seasonal trends in SO_4^{2-} concentrations within each year are attributed to seasonal active layer depths, with lower concentrations in early season attributed to shallower thaw depth and snowmelt dominated runoff (O'Donnell et al., 2012). Likewise, more pronounced increases in SO_4^{2-} and total Zn concentration in the late summer season are likely driven by seasonal active layer thickness (Barker et al., 2014; Koch et al., 2022; O'Donnell et al., 2014) that enhance groundwater interactions with sulfide minerals. Notably, the warmest winter air temperatures and highest winter snowfall regionally occurred in 2018 and 2019 (Figure S12 in Supporting Information S1), which could govern the timing of acid rock drainage intensification in the region by triggering abrupt permafrost loss and promoting soil thaw (Hamm et al., 2025; Jafarov et al., 2018; Swanson et al., 2021).

Importantly, neither watershed reached a new steady-state condition post-onset (Figure 6) but rather showed gradual decreases in SO_4^{2-} and total Zn concentrations between 2021 and 2024, indicating less acid rock drainage inputs during those years relative to 2019 and 2020. Acid-neutralizing capacity concentrations gradually increased over the same period, indicating reduced consumption of acid buffering capacity and conditions consistent with lower acid rock drainage. Together, these trends may represent a period of recovery, potentially driven by hydrologic or geological limitations on sulfide mineral oxidation (e.g., changing subsurface flow paths, talik refreezing). Several periods of relatively enhanced sulfide mineral oxidation and recovery likely took place prior to 2019 based on geochemical data from the Wulik River (e.g., in 1999–2000) (Figure S11 in Supporting Information S1) and remote sensing imagery within our study area (e.g., the Kugururok and Salmon rivers showing evidence in 2007–2008, 2012, 2018) (O'Donnell et al., 2024), although those periods seems to be minor compared to the dramatic recent shifts (Figure 6, Figure S11 in Supporting Information S1). Notwithstanding, our data indicates pronounced and concurrent onset of acid rock drainage in the summer of 2019–2020 across watersheds of the western Brooks Range and provide regional and temporal context for the chemistry our study documents in 2022 and 2023.

3.5. Implications in a Warming Arctic

Six rivers and streams in the western Brooks Range exhibited substantial changes in water chemistry due to natural acid rock drainage that coincide temporally with warm, wet periods in the region. The rivers and streams universally had sufficiently high acid-neutralizing capacity to buffer pH changes in the mainstem from acid rock drainage inputs, yet impaired tributaries exhibited pH as low as <4.0 (Figure 2b). Acidic, metal-rich seeps had more extreme water quality deterioration than natural acid rock drainage of sulfide deposits across the Brooks

2576604x, 2026, 6, Downloaded from https://agupubs.onlinelibrary.wiley.com/doi/10.1029/2026AV002407 by Jonathan O'Donnell , Wiley Online Library on [24/09/2026]. See the Terms and Conditions (https://onlinelibrary.wiley.com/terms-and-conditions) on Wiley Online Library for rules of use; OA articles are governed by the applicable Creative Commons License

Range (Graham & Kelley, 2009) (Figure 4a). Additionally, seeps differed in the metals mobilized (Figure 4b), likely due to differences in sulfide mineral source. Together, seep chemistry and metal compositional data demonstrated a high potential for water quality effects when seeps discharge directly or indirectly to adjacent surface waters. Across watersheds, point-source inputs of acid rock drainage increased the concentrations of particulate (Fe, Al, and REE) and filter-passing metals (Ni, Cd, Zn, and Mn) 3-to-21-fold downstream relative to upstream (Figure 3). Further, a synoptic sampling of the Salmon River documented increases in constituent concentrations 103 km downstream of acid rock drainage inputs of up to 70-fold in filter-passing (e.g., Ni), particulate (e.g., Fe), and both particulate and filter-passing fractions (e.g., Cd and Zn) (Figure 5). The persistence of elevated metal concentrations of this distance provides evidence that acid rock drainage associated constituents can be transported over long distances downstream. Geochemical time-series data document the abrupt onset of acid rock drainage in 2019–2020, with step-increases in SO_4^{2-} (174%–263%) and total Zn concentration (529%–769%) and decreases in acid-neutralizing capacity, followed by a multi-year recovery period of steadily decreasing SO_4^{2-} and total Zn concentrations that approached pre-onset levels (Figure 6).

Our findings highlight the sensitivity of relatively small (<2,100 km^2) Arctic watersheds to acid rock drainage that may be obscured in larger rivers that integrate processes over vast spatial scales. Increases in SO_4^{2-} concentration (Walsh et al., 2024) and load (Toohey et al., 2016; Zolkos et al., 2018) have been documented in major Arctic rivers (830,000 and 1,780,000 km^2 for the Yukon and Mackenzie Rivers, respectively) and attributed to enhanced sulfide mineral oxidation. However, major Arctic rivers have experienced gradual increases in SO_4^{2-} concentration (6%–20% per decade in the Mackenzie and Peel Rivers) and SO_4^{2-} load (~7% increase per decade in the Yukon River) that contrast with the step-increases of >200% and >700% of SO_4^{2-} and total Zn observed here (Figure 6). Yet, seasonal trends in the Yukon River show the most pronounced increases in SO_4^{2-} load occurred during August–October (Toohey et al., 2016), matching the more pronounced changes in SO_4^{2-} concentration observed here in late summer (Figures 6a and 6b). Thus, the effects of acid rock drainage in smaller watersheds akin to those studied here may be masked when evaluating changes in concentration and load at the mouth of large Arctic rivers.

The interannual dynamics of SO_4^{2-}, total Zn, and acid-neutralizing capacity within the Wulik River during onset and recovery from acid rock drainage indicate that smaller watersheds provide a critical window into the underlying processes responsible for integrated observations in the major rivers (e.g., Tank et al., 2023) influenced by many factors (e.g., precipitation, permafrost extent, groundwater flow paths, and surface vegetation). For example, the acid-neutralizing capacity of the Wulik River decreased 26% following the onset of acid rock drainage (Figure 6d), counter to the decadal increases observed in acid-neutralizing capacity of Siberian rivers (Drake et al., 2018). The underlying processes responsible for the recovery of watersheds (Figure 6) are unknown but may be controlled by finite mineral sources and/or mineral availability (Alakangas et al., 2010) or hydrologic controls of subsurface flow paths that change annually (Frey & McClelland, 2009; Koch et al., 2022; Walvoord et al., 2012). The temporal onset and recovery observed here are also in contrast to climate-driven increases in metal concentration and loads in alpine watersheds with historical mining impact (Crouch et al., 2013; Rue & McKnight, 2021) or natural acid rock drainage (Wanner et al., 2023; Zarroca et al., 2021), likely representing the interplay between permafrost thaw dynamics, mineral source limitation, and hydrologic connectivity unique to Arctic systems (Koch & O'Donnell, 2025).

Acid rock drainage across the Brooks Range has the potential to mobilize and transport metals that are toxic to downstream environments (upwards of 100 km), with potential consequences for aquatic ecosystems and rural Arctic communities (Kwong et al., 2009; Sullivan et al., 2025). With over 200 rivers and streams identified in 2025 as affected by this recent phenomenon (O'Donnell et al., 2025) and evidence here of elevated metal concentrations transported downstream of acid rock drainage inputs, we assert that acid rock drainage may pose a disproportionate threat to Arctic waterways compared to other metal release processes. This includes permafrost thaw driving enhanced release of Fe(II) and As via reductive dissolution of Fe(III) mineral (Barker et al., 2023; Patzner et al., 2020; Skierszkan et al., 2024) or Hg release from organic matter (Schuster et al., 2018; M. I. Smith et al., 2024). Here, Fe mobilization is not attributed to reductive dissolution of Fe(III) minerals, as measured (Barker et al., 2023; Patzner et al., 2020) or inferred (Sullivan et al., 2025) in other Arctic systems. Although our study design did not target low-redox environments where reductive dissolution of Fe(III) minerals is expected, geochemical indicators (e.g., SO_4^{2-}, trace metals, acid) can be used in future studies to ascertain the relative importance of Fe mobilization from sulfide mineral weathering versus Fe(III) mineral dissolution. The most mobile and notable increases were of Fe, Al, and REE in particulate and Ni, Cd, and Zn in filter-passing fractions.

2576604x, 2026, 6, Downloaded from https://agupubs.onlinelibrary.wiley.com/doi/10.1029/2026AV002407 by Jonathan O'Donnell , Wiley Online Library on [24/09/2026]. See the Terms and Conditions (https://onlinelibrary.wiley.com/terms-and-conditions) on Wiley Online Library for rules of use; OA articles are governed by the applicable Creative Commons License

Importantly, however, seeps and impaired tributaries universally have low concentrations of As, Pb, or Hg; therefore, the potential effects of acid rock drainage on As and Pb for drinking water and Hg for bioaccumulation in fish (Chételat et al., 2022) are not currently of concern. The distinct metal distributions observed in seeps across watersheds (Figure 4b) indicate that the effects of toxic metals may vary between and within watersheds as a function of host mineral composition. Therefore, mineralogical assessments could help inform future work aiming to predict the locations or severity of acid rock drainage across the Brooks Range or other regions. Further, the toxicological implications of major (e.g., Al) and trace metals (Ni, Cu, Cd, and Zn) elevated in tributaries and mainstems to fish would require modeling of metal speciation and would be influenced by the low DOC in these rivers (<2 mg L^{-1}) (Figure 2d) and concentrations of divalent cations (Figures 2g and 2h) (K. S. Smith, 2005; K. S. Smith et al., 2015), which govern metal toxicity. For example, Se concentrations of impaired tributaries exceeded the threshold set by the U.S. EPA for lotic waters (3.1 μg L^{-1}) (Figure S3d in Supporting Information S1) (U.S. EPA, 2016); however, the high SO_4^{2-} concentrations in impaired tributaries (17.6–1,820 mg L^{-1}) may decrease toxicity by reducing Se bioavailability via competition (in the form of selenate (SeO_4^{2-})) (DeForest et al., 2017). Ultimately, the negative ecological implications of this emerging Arctic disturbance will depend on the relative loading of acidic, metal rich inputs to mainstem river and the settling, remobilization, and bioavailability of metals downstream.

Sulfide mineral oxidation is a global environmental problem (Burke et al., 2018) with increasing relevance in Arctic and boreal regions (Kemeny et al., 2023; Kwong et al., 2009; O'Donnell et al., 2024, 2025; Skierszkan et al., 2026; Van Stempvoort et al., 2023) and potential to alter biogeochemical cycles within and beyond local catchments. Locally, acid rock drainage inputs may shift nutrient dynamics in otherwise oligotrophic catchments by increasing the absorption capacity of stream sediments (e.g., phosphate adsorption to Fe(III)(oxy)hydroxides) (Herndon et al., 2019), influencing hyporheic exchange (Hoagland et al., 2020), and shifting benthic metabolism (DeNicola et al., 2012). At a broader scale, sulfuric acid from sulfide mineral weathering could enhance the weathering of carbonate minerals consequently reducing the sequestration of CO_2 that occurs through carbonic acid (H_2CO_3)-driven weathering of carbonate minerals (Zolkos et al., 2018), enhancing the permafrost-carbon feedback (Walsh et al., 2024). Additional research would be needed to (a) constrain how enhanced acid rock drainage is influencing mass fluxes locally and to coastal Arctic waters, (b) quantify point versus non-point inputs (e.g., surface vs. subsurface flow paths), and (c) identify predictive landscape and climate drivers responsible for the location, timing, and magnitude of acid rock drainage development and recovery, in context of future warming scenarios and potential exacerbation by infrastructure development (Lacelle et al., 2007).

Conflict of Interest

The authors declare no conflicts of interest relevant to this study.

Availability Statement

The data are available in an associated U.S. Geological Survey Science Base data release (O'Donnell et al., 2026).

Acknowledgments

This work was supported by the USGS-NPS Water Quality Partnership Program, the USGS Changing Arctic Ecosystem Initiative of the Species Management Research Program, the NPS Arctic Inventory & Monitoring Program, the NSF (ANS-2211426), and the UC Davis Matsumara Fellowship. We thank Roman Dial and Patrick Sullivan for sample collection, Anna Maffia for laboratory assistance, Mike Rieser for data consultation, and Abagael Pruitt and Ania Szlembarska for feedback on figures and drafts. Any use of trade, firm, or product names is for descriptive purposes only and does not imply endorsement by the U.S. Government.

References

Alakangas, L., Öhlander, B., & Lundberg, A. (2010). Estimation of temporal changes in oxidation rates of sulphides in copper mine tailings at Laver, Northern Sweden. *Science of the Total Environment*, *408*(6), 1386–1392. https://doi.org/10.1016/j.scitotenv.2009.11.005

Alpers, C. N., Nordstrom, D. K., & Spitzley, J. (2003). Extreme acid mine drainage from a pyritic massive sulfide deposit: The Iron Mountain end-member. In J. L. Jambor, D. W. Blowes, & A. I. M. Ritchie (Eds.), *Environmental aspects of mine wastes* (Vol. 31, pp. 407–430). Mineralogical Association of Canada.

ANILCA Public Law. (1980). Alaska National Interest Lands Conservation Act (ANILCA), public law 96-487, 94 stat. 2371.

Antweiler, R. C. (2015). Evaluation of statistical treatments of left-censored environmental data using coincident uncensored data sets. II. Group comparisons. *Environmental Science & Technology*, *49*(22), 13439–13446. https://doi.org/10.1021/acs.est.5b02385

Baleeiro, A., Fiol, S., Otero-Fariña, A., & Antelo, J. (2018). Surface chemistry of iron oxides formed by neutralization of acidic mine waters: Removal of trace metals. *Applied Geochemistry*, *89*, 129–137. https://doi.org/10.1016/j.apgeochem.2017.12.003

Barker, A. J., Douglas, T. A., Jacobson, A. D., McClelland, J. W., Ilgen, A. G., Khosh, M. S., et al. (2014). Late season mobilization of trace metals in two small Alaskan arctic watersheds as a proxy for landscape scale permafrost active layer dynamics. *Chemical Geology*, *381*, 180–193. https://doi.org/10.1016/j.chemgeo.2014.05.012

Barker, A. J., Sullivan, T. D., Baxter, W. B., Barbato, R. A., Gallaher, S., Patton, G. E., et al. (2023). Iron oxidation–reduction processes in warming permafrost soils and surface waters expose a seasonally rusting Arctic watershed. *ACS Earth and Space Chemistry*, *7*(8), 1479–1495. https://doi.org/10.1021/acsearthspacechem.2c00367

Bau, M. (1999). Scavenging of dissolved yttrium and rare earths by precipitating iron oxyhydroxide: Experimental evidence for Ce oxidation, Y-Ho fractionation, and lanthanide tetrad effect. *Geochimica et Cosmochimica Acta*, *63*(1), 67–77. https://doi.org/10.1016/S0016-7037(99)00014-9

Burke, A., Present, T. M., Paris, G., Rae, E. C. M., Sandilands, B. H., Gaillardet, J., et al. (2018). Sulfur isotopes in rivers: Insights into global weathering budgets, pyrite oxidation, and the modern sulfur cycle. *Earth and Planetary Science Letters*, *496*, 168–177. https://doi.org/10.1016/j.epsl.2018.05.022

Carey, M. P., Koch, J. C., O'Donnell, J. A., Poulin, B. A., & Zimmerman, C. E. (2025). Linking permafrost to the abundance, biomass, and energy density of fish in Arctic headwater streams. *Ecosphere*, *16*(5), e70270. https://doi.org/10.1002/ecs2.70270

Chételat, J., McKinney, M. A., Amyot, M., Dastoor, A., Douglas, T. A., Heimbürger-Boavida, L.-E., et al. (2022). Climate change and mercury in the Arctic: Abiotic interactions. *Science of the Total Environment*, *824*, 153715. https://doi.org/10.1016/j.scitotenv.2022.153715

Clawson, C. M. (2025). Aquatic biomonitoring at red dog mine, 2024. In *Alaska department of fish and game, technical report 25-08, Fairbanks Alaska*.

Crouch, C. M., McKnight, D. M., & Todd, A. S. (2013). Quantifying sources of increasing zinc from acid rock drainage in an alpine catchment under a changing hydrologic regime. *Hydrological Processes*, *27*(5), 721–733. https://doi.org/10.1002/hyp.9650

DeCicco, L. A., Hirsch, R. M., Lorenz, D., Watkins, W. D., & Johnson, M. (2022). dataRetrieval: R packages for discovering and retrieving water data available from federal hydrologic web services, v.2.7.12. https://doi.org/10.5066/P9X4L3GE

DeForest, D. K., Brix, K. V., Elphick, J. R., Rickwood, C. J., de Bruyn, A. M. H., Tear, L. M., et al. (2017). Lentic, lotic, and sulfate-dependent waterborne selenium screening guidelines for freshwater systems. *Environmental Toxicology and Chemistry*, *36*(9), 2503–2513. https://doi.org/10.1002/etc.3793

DeNicola, D. M., Layton, L., & Czapski, T. R. (2012). Epilithic community metabolism as an indicator of impact and recovery in streams affected by acid mine drainage. *Environmental Management*, *50*(6), 1035–1046. https://doi.org/10.1007/s00267-012-9936-0

Dewitz, J., & U.S. Geological Survey (2021). National Land Cover Database (NLCD) 2019 Products (ver. 2.0, June 2021). *U.S. Geological Survey Data Release*. https://doi.org/10.5066/P9KZCM54

Drake, T. W., Tank, S. E., Zhulidov, A. V., Holmes, R. M., Gurtovaya, T., & Spencer, R. G. M. (2018). Increasing alkalinity export from large Russian arctic Rivers. *Environmental Science & Technology*, *52*(15), 8302–8308. https://doi.org/10.1021/acs.est.8b01051

Elberling, B. (2005). Temperature and oxygen control on pyrite oxidation in frozen mine tailings. *Cold Regions Science and Technology*, *41*(2), 121–133. https://doi.org/10.1016/j.coldregions.2004.09.004

Ficklin, W. H., Plumlee, G. S., Smith, K. S., & McHugh, J. B. (1992). Geochemical classification of mine drainages and natural drainages in mineralized areas. In *Presented at International Symposium on water-rock interaction conference, Park City, Utah* (pp. 381–384).

Frey, K. E., & McClelland, J. W. (2009). Impacts of permafrost degradation on arctic river biogeochemistry. *Hydrological Processes*, *23*(1), 169–182. https://doi.org/10.1002/hyp.7196

Gao, L., Zhou, Z., Reyes, A. V., & Guo, L. (2018). Yields and characterization of dissolved organic matter from different aged soils in Northern Alaska. *Journal of Geophysical Research: Biogeosciences*, *123*(7), 2035–2052. https://doi.org/10.1029/2018JG004408

Gault, K. B., Gammon, P., & Fortin, D. (2015). A geochemical characterization of cold-water natural acid rock drainage at the Zn–Pb XY deposit, Yukon, Canada. *Applied Geochemistry*, *62*, 35–47. https://doi.org/10.1016/j.apgeochem.2015.06.003

Google LLC. (2024). Google Earth Pro, Version 7.3.7.

Graham, G. E., & Kelley, K. D. (2009). The Drenchwater deposit, Alaska: An example of a natural low pH environment resulting from weathering of an undisturbed shale-hosted Zn–Pb–Ag deposit. *Applied Geochemistry*, *24*(2), 232–245. https://doi.org/10.1016/j.apgeochem.2008.11.016

Hamm, A., Schytt Mannerfelt, E., Mohammed, A. A., Painter, S. L., Coon, E. T., & Frampton, A. (2025). Model-based analysis of solute transport and potential carbon mineralization in the active layer of a hillslope underlain by permafrost with seasonal variability and climate change. *The Cryosphere*, *19*(9), 3693–3724. https://doi.org/10.5194/tc-19-3693-2025

Hem, J. D. (1963). Chemical equilibria and rates of manganese oxidation: U.S. Geological Survey Water Supply Paper 1667, iv, 24 cm (p. 64). https://doi.org/10.3133/wsp1667A

Herndon, E. M., Kinsman-Costello, L., Duroe, K. A., Mills, J., Kane, E. S., Sebestyen, S. D., et al. (2019). Iron (oxyhydr)oxides serve as phosphate traps in tundra and boreal peat soils. *Journal of Geophysical Research: Biogeosciences*, *124*(2), 227–246. https://doi.org/10.1029/2018JG004776

Hoagland, B., Navarre-Sitchler, A., Cowie, R., & Singha, K. (2020). Groundwater–Stream connectivity mediates metal(loid) geochemistry in the hyporheic zone of streams impacted by historic mining and acid rock drainage. *Frontiers in Water*, *2*, 600409. https://doi.org/10.3389/frwa.2020.600409

Jafarov, E. E., Coon, E. T., Harp, D. R., Wilson, C. J., Painter, S. L., Atchley, A. L., & Romanovsky, V. E. (2018). Modeling the role of preferential snow accumulation in through talik development and hillslope groundwater flow in a transitional permafrost landscape. *Environmental Research Letters*, *13*(10), 105006. https://doi.org/10.1088/1748-9326/aadd30

Jorgenson, T., Yoshikawa, K., Kanevskiy, M., Shur, Y., Romanovsky, V., Marchenko, S., et al. (2008). Permafrost characteristics of Alaska. In D. L. Kane & K. M. Hinkel (Eds.), *Proceedings of the ninth international conference on Permafrost: Fairbanks, Alaska, Institute of Northern Engineering* (pp. 121–122). University of Alaska Fairbanks.

Kelley, K. D., & Jennings, S. (2004). A special issue devoted to barite and Zn–Pb–Ag deposits in the red dog district, Western brooks range, Northern Alaska. *Economic Geology*, *99*(7), 1267–1280. https://doi.org/10.2113/gsecongeo.99.7.1267

Kelley, K. D., & Taylor, C. D. (1997). Environmental geochemistry of shale-hosted Ag Pb Zn massive sulfide deposits in northwest Alaska: Natural background concentrations of metals in water from mineralized areas. *Applied Geochemistry*, *12*(4), 397–409. https://doi.org/10.1016/S0883-2927(97)00009-7

Kemeny, P. C., Li, G. K., Douglas, M., Berelson, W., Chadwick, A. J., Dalleska, N. F., et al. (2023). Arctic permafrost thawing enhances sulfide oxidation. *Global Biogeochemical Cycles*, *37*(11), e2022GB007644. https://doi.org/10.1029/2022GB007644

Kemeny, P. C., Lopez, G. I., Dalleska, N. F., Torres, M., Burke, A., Bhatt, M. P., et al. (2021). Sulfate sulfur isotopes and major ion chemistry reveal that pyrite oxidation counteracts CO_2 drawdown from silicate weathering in the Langtang-Trisuli-Narayani River system, Nepal Himalaya. *Geochimica et Cosmochimica Acta*, *294*, 43–69. https://doi.org/10.1016/j.gca.2020.11.009

Kimball, B. A., Runkel, R. L., Walton-Day, K., & Bencala, K. E. (2002). Assessment of metal loads in watersheds affected by acid mine drainage by using tracer injection and synoptic sampling: Cement Creek, Colorado, USA. *Applied Geochemistry*, *17*(9), 1183–1207. https://doi.org/10.1016/S0883-2927(02)00017-3

Kirby, C. S., Thomas, H. M., Southam, G., & Donald, R. (1999). Relative contributions of abiotic and biological factors in Fe(II) oxidation in mine drainage. *Applied Geochemistry*, *14*(4), 511–530. https://doi.org/10.1016/S0883-2927(98)00071-7

Koch, J. C., & O'Donnell, J. A. (2025). Observing Northern high-latitude River systems to understand changes in a warming arctic. *Current Climate Change Reports*, *11*(1), 5. https://doi.org/10.1007/s40641-025-00202-5

Koch, J. C., Sjöberg, Y., O'Donnell, J. A., Carey, M. P., Sullivan, P. F., & Terskaia, A. (2022). Sensitivity of headwater streamflow to thawing permafrost and vegetation change in a warming Arctic. *Environmental Research Letters*, *17*(4), 044074. https://doi.org/10.1088/1748-9326/ac5f2d

25776604x, 2026, 6, Downloaded from https://agupubs.onlinelibrary.wiley.com/doi/10.1029/2026AV002407 by Jonathan O'Donnell , Wiley Online Library on [24/09/2026]. See the Terms and Conditions (https://onlinelibrary.wiley.com/terms-and-conditions) on Wiley Online Library for rules of use; OA articles are governed by the applicable Creative Commons License

Kwong, Y. T. J., Whitley, G., & Roach, P. (2009). Natural acid rock drainage associated with black shale in the Yukon Territory, Canada. *Applied Geochemistry*, *24*(2), 221–231. https://doi.org/10.1016/j.apgeochem.2008.11.017

Lacelle, D., Doucet, A., Clark, I. D., & Lauriol, B. (2007). Acid drainage generation and seasonal recycling in disturbed permafrost near Eagle Plains, northern Yukon Territory, Canada. *Chemical Geology*, *243*(1–2), 157–177. https://doi.org/10.1016/j.chemgeo.2007.05.021

Lehn, G. O., Jacobson, A. D., Douglas, T. A., McClelland, J. W., Barker, A. J., & Khosh, M. S. (2017). Constraining seasonal active layer dynamics and chemical weathering reactions occurring in North Slope Alaskan watersheds with major ion and isotope ($\delta^{34}S$ SO_4, $\delta^{13}C$ DIC, $^{87}Sr/^{86}Sr$, $\delta^{44}/^{40}Ca$, and $\delta^{44}/^{42}Ca$) measurements. *Geochimica et Cosmochimica Acta*, *217*, 399–420. https://doi.org/10.1016/j.gca.2017.07.042

Loiko, S. V., Pokrovsky, O. S., Raudina, T. V., Lim, A., Kolesnichenko, L. G., Shirokova, L. S., et al. (2017). Abrupt permafrost collapse enhances organic carbon, CO_2, nutrient and metal release into surface waters. *Chemical Geology*, *471*, 153–165. https://doi.org/10.1016/j.chemgeo.2017.10.002

Manning, A. H., Petach, T. N., Runkel, R. L., & McKnight, D. M. (2024). Climate-Driven increases in stream metal concentrations in mineralized watersheds throughout the Colorado rocky Mountains, USA. *Water Resources Research*, *60*(4), e2023WR036062. https://doi.org/10.1029/2023wr036062

Morgan, B., & Lahav, O. (2007). The effect of pH on the kinetics of spontaneous Fe(II) oxidation by O_2 in aqueous solution – Basic principles and a simple heuristic description. *Chemosphere*, *68*(11), 2080–2084. https://doi.org/10.1016/j.chemosphere.2007.02.015

Munk, L., Faure, G., Pride, D. E., & Bigham, J. M. (2002). Sorption of trace metals to an aluminum precipitate in a stream receiving acid rock-drainage; Snake River, Summit County, Colorado. *Applied Geochemistry*, *17*(4), 421–430. https://doi.org/10.1016/S0883-2927(01)00098-1

Nordstrom, D. K. (2000). Advances in the hydrogeochemistry and microbiology of acid mine waters. *International Geology Review*, *42*(6), 499–515. https://doi.org/10.1080/00206810009465095

Nordstrom, D. K. (2011). Mine waters: Acidic to circumneutral. *Elements*, *7*(6), 393–398. https://doi.org/10.2113/gselements.7.6.393

Nordstrom, D. K., & Alpers, C. (1999). Geochemistry of acid mine waters. In G. S. Plumlee & M. J. Logsdon (Eds.) *The environmental geochemistry of mineral deposits. Part A. Processes, methods, and health issues* (Vol. 6, pp. 133–160). Society for Economic Geologists.

O'Donnell, J. A., Aiken, G. R., Swanson, D. K., Panda, S., Butler, K. D., & Baltensperger, A. P. (2016). Dissolved organic matter composition of Arctic rivers: Linking permafrost and parent material to riverine carbon. *Global Biogeochemical Cycles*, *30*(12), 1811–1826. https://doi.org/10.1002/2016GB005482

O'Donnell, J. A., Aiken, G. R., Walvoord, M. A., & Butler, K. D. (2012). Dissolved organic matter composition of winter flow in the Yukon River basin: Implications of permafrost thaw and increased groundwater discharge. *Global Biogeochemical Cycles*, *26*(4), 2012GB004341. https://doi.org/10.1029/2012GB004341

O'Donnell, J. A., Aiken, G. R., Walvoord, M. A., Raymond, P. A., Butler, K. D., Dornblaser, M. M., & Heckman, K. (2014). Using dissolved organic matter age and composition to detect permafrost thaw in boreal watersheds of interior Alaska. *Journal of Geophysical Research: Biogeosciences*, *119*(11), 2155–2170. https://doi.org/10.1002/2014JG002695

O'Donnell, J. A., Carey, M. P., Koch, J. C., Baughman, C., Hill, K., Evinger, T., et al. (2025). Rusting Rivers: Assessing the causes and consequences in Alaska and across the Arctic. In *Arctic report card 2025, rusting Rivers: Assessing the causes and consequences in Alaska and across the Arctic—NOAA Arctic*. https://doi.org/10.25923/f3tr-5759

O'Donnell, J. A., Carey, M. P., Koch, J. C., Baughman, C., Hill, K., Zimmerman, C. E., et al. (2024). Metal mobilization from thawing permafrost to aquatic ecosystems is driving rusting of Arctic streams. *Communications Earth & Environment*, *5*(1), 268. https://doi.org/10.1038/s43247-024-01446-z

O'Donnell, J. A., Carey, M. P., Koch, J. C., Xu, X., Poulin, B. A., Walker, J., & Zimmerman, C. E. (2020). Permafrost hydrology drives the assimilation of old carbon by stream food webs in the Arctic. *Ecosystems*, *23*(2), 435–453. https://doi.org/10.1007/s10021-019-00413-6

O'Donnell, J. A., Koch, J. C., Carey, M. P., Poulin, B. A., Evinger, T. G., Frei, R., & Pruitt, A. (2026). Chemical composition of water in lakes, ponds, rivers, and creeks in northwest Alaska [Dataset]. *U.S. Geological Survey data release*. https://doi.org/10.5066/P13EV8UD

Patzner, M. S., Mueller, C. W., Malusova, M., Baur, M., Nikeleit, V., Scholten, T., et al. (2020). Iron mineral dissolution releases iron and associated organic carbon during permafrost thaw. *Nature Communications*, *11*(1), 6329. https://doi.org/10.1038/s41467-020-20102-6

Plumlee, G. S. (1997). The environmental geology of mineral deposits. In G. S. Plumlee, M. J. Logsdon, & L. F. Filipek (Eds.) *The environmental geochemistry of mineral deposits* (pp. 71–116). Society of Economic Geologists. https://doi.org/10.5382/Rev.06.03

Rantanen, M., Karpechko, A. Y., Lipponen, A., Nordling, K., Hyvärinen, O., Ruosteenoja, K., et al. (2022). The Arctic has warmed nearly four times faster than the globe since 1979. *Communications Earth & Environment*, *3*(1), 168. https://doi.org/10.1038/s43247-022-00498-3

R Core Team. (2025). *R: A language and environment for statistical computing*. R Foundation for Statistical Computing. Retrieved from https://www.R-project.org/

Rember, R. D., & Trefry, J. H. (2004). Increased concentrations of dissolved trace metals and organic carbon during snowmelt in rivers of the Alaskan arctic. *Geochimica et Cosmochimica Acta*, *68*(3), 477–489. https://doi.org/10.1016/S0016-7037(03)00458-7

Rounds, S. A., & Wilde, F. D. (2012). Chapter A6. Section 6.6. Alkalinity and acid neutralizing capacity. In *National field manual for the collection of water-quality data (techniques of Water-Resources Investigations, Book 9, Chapter A6.6)*. U.S. Geological Survey. https://doi.org/10.3133/twri09A6.6

Rue, G., & McKnight, D. M. (2021). Enhanced rare Earth element mobilization in a Mountain watershed of the Colorado mineral Belt with concomitant detection in aquatic biota: Increasing climate change-driven degradation to water quality. *Environmental Science & Technology*, *55*(21), 14378–14388. https://doi.org/10.1021/acs.est.1c02958

Schippers, A., & Sand, W. (1999). Bacterial leaching of metal sulfides proceeds by two indirect mechanisms via thiosulfate or via polysulfides and sulfur. *Applied and Environmental Microbiology*, *65*(1), 319–321. https://doi.org/10.1128/AEM.65.1.319-321.1999

Schmidt, J. M. (1997). Shale-Hosted Zn-Pb-Ag and barite deposits of Alaska. In R. J. Goldfarb & L. D. Miller (Eds) *Mineral deposits of Alaska* (pp. 35–65). Society of Economic Geologists. https://doi.org/10.5382/Mono.09.03

Schuster, P. F., Schaefer, K. M., Aiken, G. R., Antweiler, R. C., Dewild, J. F., Gryziec, J. D., et al. (2018). Permafrost stores a globally significant amount of Mercury. *Geophysical Research Letters*, *45*(3), 1463–1471. https://doi.org/10.1002/2017GL075571

Schuster, P. F., Striegl, R. G., Aiken, G. R., Krabbenhoft, D. P., Dewild, J. F., Butler, K., et al. (2011). Mercury export from the Yukon River Basin and potential response to a changing climate. *Environmental Science & Technology*, *45*(21), 9262–9267. https://doi.org/10.1021/es202068b

Schuur, E. A. G., McGuire, A. D., Schädel, C., Grosse, G., Harden, J. W., Hayes, D. J., et al. (2015). Climate change and the permafrost carbon feedback. *Nature*, *520*(7546), 171–179. https://doi.org/10.1038/nature14338

Sherlock, E. J., Lawrence, R. W., & Poulin, R. (1995). On the neutralization of acid rock drainage by carbonate and silicate minerals. *Environmental Geology*, *25*(1), 43–54. https://doi.org/10.1007/BF01061829

Shogren, A. J., Zarnetske, J. P., Abbott, B. W., Bratsman, S., Brown, B., Carey, M. P., et al. (2022). Multi-year, spatially extensive, watershed-scale synoptic stream chemistry and water quality conditions for six permafrost-underlain Arctic watersheds. *Earth System Science Data*, *14*(1), 95–116. https://doi.org/10.5194/essd-14-95-2022

2576604x, 2026, 6, Downloaded from https://agupubs.onlinelibrary.wiley.com/doi/10.1029/2026AV002407 by Jonathan O'Donnell , Wiley Online Library on [24/09/2026]. See the Terms and Conditions (https://onlinelibrary.wiley.com/terms-and-conditions) on Wiley Online Library for rules of use; OA articles are governed by the applicable Creative Commons License

Short, T. M., Black, J. A., & Birge, W. J. (1990). Effects of acid-mine drainage on the chemical and biological character of an alkaline headwater stream. *Archives of Environmental Contamination and Toxicology*, *19*(2), 241–248. https://doi.org/10.1007/BF01056093

Skierszkan, E. K., Carey, S. K., Jackson, S. I., Fellwock, M., Fraser, C., & Lindsay, M. B. J. (2024). Seasonal controls on stream metal(loid) signatures in mountainous discontinuous permafrost. *Science of the Total Environment*, *908*, 167999. https://doi.org/10.1016/j.scitotenv.2023.167999

Skierszkan, E. K., Szeitz, A. J., Lindsay, M. B. J., & Carey, S. K. (2026). Abrupt stream acidification and metal mobilization from permafrost degradation. *Science*, *392*(6800), 863–867. https://doi.org/10.1126/science.aea2898

Smith, K. S. (2005). Use of the biotic ligand model to predict metal toxicity to aquatic biota in areas of differing geology. *Journal American Society of Mining and Reclamation*, *2005*(1), 1134–1155. https://doi.org/10.21000/jasmr05011134

Smith, K. S., Balistrieri, L. S., & Todd, A. S. (2015). Using biotic ligand models to predict metal toxicity in mineralized systems. *Applied Geochemistry*, *57*, 55–72. https://doi.org/10.1016/j.apgeochem.2014.07.005

Smith, M. I., Ke, Y., Geyman, E. C., Reahl, J. N., Douglas, M. M., Seelen, E. A., et al. (2024). Mercury stocks in discontinuous permafrost and their mobilization by river migration in the Yukon River Basin. *Environmental Research Letters*, *19*(8), 084041. https://doi.org/10.1088/1748-9326/ad536e

Smith, S. L., O'Neill, H. B., Isaksen, K., Noetzli, J., & Romanovsky, V. E. (2022). The changing thermal state of permafrost. *Nature Reviews Earth & Environment*, *3*(1), 10–23. https://doi.org/10.1038/s43017-021-00240-1

Strauss, J., Schirrmeister, L., Grosse, G., Fortier, D., Hugelius, G., Knoblauch, C., et al. (2017). Deep Yedoma permafrost: A synthesis of depositional characteristics and carbon vulnerability. *Earth-Science Reviews*, *172*, 75–86. https://doi.org/10.1016/j.earscirev.2017.07.007

Sullivan, P. F., Dial, R. J., Cooper, D. J., Diamond, C., Tino, C. J., Gregory, D. D., et al. (2025). Wild, scenic, and toxic: Recent degradation of an iconic Arctic watershed with permafrost thaw. *Proceedings of the National Academy of Sciences*, *122*(37), e2425644122. https://doi.org/10.1073/pnas.2425644122

Swanson, D. K., Sousanes, P. J., & Hill, K. (2021). Increased mean annual temperatures in 2014–2019 indicate permafrost thaw in Alaskan national parks. *Arctic Antarctic and Alpine Research*, *53*(1), 1–19. https://doi.org/10.1080/15230430.2020.1859435

Tank, S. E., McClelland, J. W., Spencer, R. G. M., Shiklomanov, A. I., Suslova, A., Moatar, F., et al. (2023). Recent trends in the chemistry of major northern rivers signal widespread Arctic change. *Nature Geoscience*, *16*(9), 789–796. https://doi.org/10.1038/s41561-023-01247-7

Thomas, P. A., Blaskey, D., Cheng, Y., Carey, M. P., Swanson, H. K., Newman, A. J., et al. (2025). Warming Alaskan rivers affect first-year growth in critical northern food fishes. *Scientific Reports*, *15*(1), 28834. https://doi.org/10.1038/s41598-025-14711-8

To, T. B., Nordstrom, D. K., Cunningham, K. M., Ball, J. W., & McCleskey, R. B. (1999). New method for the direct determination of dissolved Fe(III) concentration in acid mine waters. *Environmental Science & Technology*, *33*(5), 807–813. https://doi.org/10.1021/es980684z

Todd, A. S., Manning, A. H., Verplanck, P. L., Crouch, C., McKnight, D. M., & Dunham, R. (2012). Climate-change-driven deterioration of water quality in a mineralized watershed. *Environmental Science & Technology*, *46*(17), 9324–9332. https://doi.org/10.1021/es3020056

Toohey, R. C., Herman-Mercer, N. M., Schuster, P. F., Mutter, E. A., & Koch, J. C. (2016). Multidecadal increases in the Yukon River Basin of chemical fluxes as indicators of changing flowpaths, groundwater, and permafrost. *Geophysical Research Letters*, *43*(23), 12,120–12,130. https://doi.org/10.1002/2016GL070817

U.S. Environmental Protection Agency. (1994). Method 200.7: Determination of metals and trace elements in water and wastes by inductively coupled plasma-atomic emission spectrometry (revision 4.4).

U.S. Environmental Protection Agency. (1998). Method 6020A (SW-846): Inductively coupled plasma-mass spectrometry (revision 1).

U.S. Environmental Protection Agency. (2002). Method 1631, revision E: Mercury in water by oxidation, purge and trap, and cold vapor atomic fluorescence spectrometry (EPA-821-R-02-019).

U.S. Environmental Protection Agency. (2007). Method 3015A: Microwave-assisted acid digestion of aqueous samples and extracts (revision 1).

U.S. Environmental Protection Agency. (2016). *Aquatic life ambient water quality criterion for Selenium—Freshwater 2016, EPA 822-R-16-006*. Office of Water.

U.S. Geological Survey. (2025). USGS water data for the Nation: U.S. Geological Survey national water information System database. https://doi.org/10.5066/F7P55KJN

Van Stempvoort, D. R., Spoelstra, J., Bickerton, G., Koehler, G., Mayer, B., Nightingale, M., & Miller, J. (2023). Sulfate in streams and groundwater in a cold region (Yukon Territory, Canada): Evidence of weathering processes in a changing climate. *Chemical Geology*, *631*, 121510. https://doi.org/10.1016/j.chemgeo.2023.121510

Verplanck, P. L., Nordstrom, D. K., Taylor, H. E., & Kimball, B. A. (2004). Rare earth element partitioning between hydrous ferric oxides and acid mine water during iron oxidation. *Applied Geochemistry*, *19*(8), 1339–1354. https://doi.org/10.1016/j.apgeochem.2004.01.016

Walsh, E. V., Hilton, R. G., Tank, S. E., & Amos, E. (2024). Temperature sensitivity of the mineral permafrost feedback at the continental scale. *Science Advances*, *10*(41), eadq4893. https://doi.org/10.1126/sciadv.adq4893

Walvoord, M. A., Voss, C. I., & Wellman, T. P. (2012). Influence of permafrost distribution on groundwater flow in the context of climate-driven permafrost thaw: Example from Yukon Flats Basin, Alaska, United States. *Water Resources Research*, *48*(7), W07524. https://doi.org/10.1029/2011WR011595

Wanner, C., Moradi, H., Ingold, P., Cardenas Bocanegra, M. A., Mercurio, R., & Furrer, G. (2023). Rock glaciers in the Central Eastern Alps—How permafrost degradation can cause acid rock drainage, mobilization of toxic elements and formation of basaluminite. *Global and Planetary Change*, *227*, 104180. https://doi.org/10.1016/j.gloplacha.2023.104180

Wilson, F. H., Hults, C. P., Mull, C. G., & Karl, S. M. (2015). Geologic map of Alaska: U.S. Geological Survey Scientific Investigations Map 3340. https://doi.org/10.3133/SIM3340

Zarroca, M., Roqué, C., Linares, R., Salminci, J. G., & Gutiérrez, F. (2021). Natural acid rock drainage in alpine catchments: A side effect of climate warming. *Science of the Total Environment*, *778*, 146070. https://doi.org/10.1016/j.scitotenv.2021.146070

Zolkos, S., Tank, S. E., & Kokelj, S. V. (2018). Mineral weathering and the permafrost carbon-climate feedback. *Geophysical Research Letters*, *45*(18), 9623–9632. https://doi.org/10.1029/2018GL078748

References From the Supporting Information

Kassambara, A. (2023). Rstatix: Pipe-friendly framework for basic statistical tests. *R package version 0.7.2*. Retrieved from https://rpkgs.datanovia.com/rstatix/

Piper, A. M. (1944). A graphic procedure in the geochemical interpretation of water-analyses. *EOS Transactions of the American Geophysical Union*, *25*(6), 914–928.

2576604x, 2026, 6, Downloaded from https://agupubs.onlinelibrary.wiley.com/doi/10.1029/2026AV002407 by Jonathan O'Donnell , Wiley Online Library on [24/09/2026]. See the Terms and Conditions (https://onlinelibrary.wiley.com/terms-and-conditions) on Wiley Online Library for rules of use; OA articles are governed by the applicable Creative Commons License